antibiotics

MDPI

Article

Antibacterial and Biofilm-Targeting Performance of Cefuroxime Axetil-Loaded Eudragit® Nanoparticles

Pervin Soyer [1], Tilbe Çevikelli [2], Umay Merve Güven Bölgen [3] and A. Alper Öztürk [4,*]

[1] Department of Pharmaceutical Microbiology, Faculty of Pharmacy, Anadolu University, 26470 Eskişehir, Türkiye; pervinsoyer@anadolu.edu.tr
[2] Department of Pharmaceutical Technology, Faculty of Pharmacy, Bahçeşehir University, 34349 İstanbul, Türkiye; tilbe.cevikelli@bau.edu.tr
[3] Department of Pharmaceutical Technology, Faculty of Pharmacy, Çukurova University, 01330 Adana, Türkiye; umaymerveguven@gmail.com
[4] Department of Pharmaceutical Technology, Faculty of Pharmacy, Anadolu University, 26470 Eskişehir, Türkiye
* Correspondence: aaozturk@anadolu.edu.tr

Abstract

Background/Objectives: Cefuroxime axetil (CA) is a poorly water-soluble second-generation cephalosporin. This study aimed to develop CA-loaded Eudragit® RS100/RL100 nanoparticles (NPs) and investigate the influence of polymer composition and drug-to-polymer ratio on their physicochemical, antibacterial, and antibiofilm properties. **Methods:** Six CA-loaded NPs (NP-1–NP-6) were prepared using nano spray drying with Eudragit® RS100, RL100, or their 1:1 mixture at drug-to-polymer ratios of 1:1 and 1:2. Particle characteristics, drug content, and structural properties were evaluated. Antibacterial activity was assessed using agar well diffusion, broth microdilution, and time-kill assays, while antibiofilm activity against pre-established *Staphylococcus aureus* and *Escherichia coli* biofilms was determined using crystal violet staining. Additional analyses included drug-content-normalized MIC, MIC-normalized time-kill exposure, and concentration–response area under the curve (AUC). **Results:** All drug-loaded NPs retained antibacterial activity and reduced established biofilm biomass, whereas blank NPs showed no detectable activity. FT-IR and ^{1}H-NMR analyses indicated no evidence of new covalent interactions. Free CA exhibited greater planktonic antibacterial potency, including after drug-content normalization. Among the NPs, NP-1 showed the most favorable MIC profile, while MIC-normalized time-kill analysis revealed NP-dependent exposure differences without consistent bactericidal activity. At 500 µg/mL, all CA-loaded NPs reduced biofilm biomass by more than 95% against both bacterial species. NP-6 exhibited the highest numerical antibiofilm AUC values against *S. aureus* (133.37) and *E. coli* (128.85), although these differences were descriptive and did not establish statistical superiority. **Conclusions:** CA-loaded Eudragit® NPs demonstrated formulation-dependent antibacterial and antibiofilm responses, with NP-1 performing favorably in planktonic inhibition and NP-6 in integrated biofilm biomass reduction. These findings support further investigation of Eudragit®-based antibiotic delivery systems, although superiority over free CA and therapeutic advantages remain unverified.

Keywords: Cefuroxime axetil; Eudragit® RS 100; Eudragit® RL 100; nanoparticles; nano spray drying; antibacterial activity; biofilm; time-kill assay; antimicrobial drug delivery

Check for updates

Academic Editors: Manuel Simões, Jordi Vila, Nicholas Dixon and Marc Maresca

Received: 23 September 2026
Revised: 30 October 2026
Accepted: 3 November 2026
Published: 12 November 2026

Copyright: © 2026 by the authors. Licensee MDPI, Basel, Switzerland. This article is an open access article distributed under the terms and conditions of the Creative Commons Attribution (CC BY) license.

1. Introduction

The increasing prevalence of difficult-to-treat bacterial infections and the persistence of biofilm-associated microorganisms remain major challenges in antimicrobial therapy.

Beyond antimicrobial resistance, the effectiveness of conventional antibiotics may be limited by poor aqueous solubility, instability, and unfavorable drug-delivery characteristics. Polymeric nanoparticles (NPs) have therefore attracted attention as carriers capable of modifying drug availability and interactions with biological environments. However, their potential advantages depend on NP characteristics and require experimental validation [1–3]. The properties of antibiotic-loaded NPs can be tailored by adjusting polymer composition, drug-to-polymer ratio, particle size, and surface characteristics. Although nanoencapsulation may protect drugs and modify their release behavior, improved antimicrobial potency or biofilm penetration cannot be assumed solely from particle formation. These outcomes depend on the NP, drug-release characteristics, and interactions with bacterial cells and biofilm components [1,2,4–9].

Eudragit® RS 100 (ERS 100) and Eudragit® RL 100 (ERL 100) are water-insoluble ammonio methacrylate copolymers widely used in pharmaceutical delivery systems. Their different quaternary ammonium group contents result in distinct permeability characteristics, with ERL 100 generally exhibiting greater permeability than ERS 100. Combining these polymers provides an opportunity to investigate the influence of matrix composition on drug incorporation and NP performance [10,11]. Their solubility in ethanol also permits processing with cefuroxime axetil (CA) using nano spray drying without an emulsification step. Furthermore, their positively charged groups may influence interactions with bacterial surfaces and biofilm components, although these interactions do not necessarily translate into improved antimicrobial efficacy. The manufacturing method also affects NP characteristics [12]. Spray drying offers a relatively rapid, single-step approach to producing dry particulate NPs [13–15]. The Nano Spray Dryer (Buchi B-90) employs vibrating-mesh atomization and electrostatic particle collection, enabling the recovery of submicron particles from small feed volumes. Formulation and processing conditions can influence particle size, drug incorporation, and other physicochemical characteristics [16–25].

The incorporation of antibiotics into polymeric NPs has emerged as a promising strategy to improve drug delivery and potentially enhance antimicrobial performance. Previous studies have demonstrated that nanoparticulate carriers may protect encapsulated antibiotics from degradation, modulate drug release, and improve their localization within bacterial biofilms, thereby enhancing antibacterial or antibiofilm activity under specific experimental conditions. However, these benefits are strongly dependent on the physicochemical properties of the carrier, drug-loading characteristics, release behavior, and the susceptibility of the target microorganism. Importantly, improved antibiofilm performance does not necessarily correspond to lower minimum inhibitory concentrations (MICs) against planktonic bacteria. Therefore, evaluating antibiotic-loaded NPs using complementary microbiological assays is essential to distinguish their effects on planktonic bacterial growth from their activity against established biofilms [26,27].

CA is an orally administered ester prodrug of cefuroxime, a second-generation cephalosporin antibiotic that inhibits bacterial cell wall synthesis following conversion to its active form. Despite its established antibacterial activity, CA exhibits poor aqueous solubility and variable oral bioavailability, motivating research into alternative pharmaceutical formulations [28–34]. The incorporation of antibiotics into polymeric NPs has been investigated as a strategy to modulate drug release, improve drug stability, and potentially enhance antimicrobial delivery to bacterial biofilms. Previous studies have demonstrated that nanoparticulate delivery systems can improve antibacterial or antibiofilm performance under specific experimental conditions, although these effects depend on the physicochemical properties of the carrier, drug availability, and the target microorganism [26,27]. Nevertheless, incorporation into a polymeric carrier does not necessarily improve immediate antibacterial potency, because drug availability may depend on release from the formulation.

Consequently, the value of CA-loaded NPs should be assessed through their physicochemical characteristics and experimentally demonstrated microbiological performance rather than an assumed superiority over free CA [2]. Although Eudragit®-based systems have been investigated for drug delivery, comparative evidence linking ERS 100/ERL 100 composition and drug-to-polymer ratio with the microbiological performance of nano-spray-dried CA-NPs remains limited [35–37]. The potential application of antibiotic-loaded NPs against bacterial biofilms is particularly relevant because the extracellular polymeric matrix can restrict antimicrobial transport and contribute to reduced antibiotic susceptibility. Polymeric nanocarriers may influence drug distribution and interactions within biofilm environments; however, their effectiveness depends on particle dimensions, surface properties, aggregation, and interactions with the extracellular matrix [26,27]. Biofilm-associated applications also require particular caution, because NP penetration and retention depend on particle dimensions, surface properties, aggregation, and interactions with the extracellular matrix. Accordingly, reduced biofilm biomass cannot independently establish enhanced penetration, bacterial killing, or biofilm eradication [38]. Therefore, this study aimed to prepare CA-loaded NPs using ERS 100, ERL 100, and their combination at different drug-to-polymer ratios through nano spray drying. The NPs were evaluated for particle size, polydispersity index, zeta potential, drug content, incorporation efficiency, and structural characteristics using FT-IR and ^{1}H-NMR analyses. Antibacterial activity was investigated against *Bacillus subtilis*, *Staphylococcus aureus*, and *Escherichia coli* using agar diffusion and broth microdilution assays, while time-kill kinetics and effects on pre-established biofilm biomass were evaluated for *S. aureus* and *E. coli*. The primary objective was to determine how polymer composition influences NP characteristics and microbiological performance, rather than to presume superior antibacterial activity relative to free CA.

2. Results and Discussion

CA is a poorly water-soluble ester prodrug of cefuroxime, and its pharmaceutical performance is limited in part by dissolution-dependent and variable absorption. Previous formulation approaches, including solid dispersions, nanoemulsions, and self-nanoemulsifying systems, have therefore attempted to improve its solubilization and delivery characteristics. In the present study, the use of ERS 100 and ERL 100 extended this formulation concept to polymeric nano-sized carriers produced by Nano Spray Dryer B-90. The suitability of Eudragit polymers for particulate drug-delivery systems is well established, and differences in their functional quaternary ammonium group content can influence hydration, permeability, drug diffusion, surface properties, and ultimately release behavior [11,39,40]. Earlier work with ciprofloxacin-loaded ERS 100/ERL 100-containing NPs also demonstrated that Eudragit composition can affect NP characteristics and permit prolonged antibiotic release while preserving antibacterial activity [41]. Nevertheless, because drug-release kinetics were not directly determined in the present study, differences among the current NPs should be interpreted as being consistent with polymer-dependent drug availability rather than direct evidence of sustained or controlled release.

2.1. Validation of the UV-Visible Spectrophotometric Method for CA Quantification

The UV-visible spectrophotometric method developed for the quantitative determination of CA was validated in methanol:water (3:2, *v*/*v*) in terms of linearity, precision, accuracy, limit of detection (LOD), and limit of quantification (LOQ). CA was analyzed at 278 nm over a concentration range of 2.5–17.5 µg/mL. The calibration curve showed a strong linear relationship between CA concentration and absorbance within the investigated range, with the regression equation $y = 0.0385x + 0.0424$ and a coefficient of determination ($R^2 = 0.9993$). The LOD and LOQ were calculated as 0.4 and 1.3 µg/mL, respectively. The

LOQ was below the lowest concentration of the calibration range (2.5 µg/mL), confirming adequate analytical sensitivity within the selected working range. Method precision was evaluated at three concentration levels (7.5, 10.0, and 12.5 µg/mL) over three consecutive days. The relative standard deviation (%RSD) values ranged from 0.2% to 1.4%, demonstrating low intra- and interday variability. Accuracy was assessed by recovery analysis at the same three concentration levels. Individual recovery values ranged from 99.0% to 101.2%, while the mean recoveries were 99.4%, 99.7%, and 100.2% at 7.5, 10.0, and 12.5 µg/mL, respectively. The %RSD values for the recovery measurements ranged from 0.5% to 0.9%. Recovery was calculated as the ratio of the concentration found, obtained from the regression equation to the nominal concentration (x100); individual values slightly above 100% therefore reflect random analytical variability, and all individual values were within the commonly accepted range of 98–102%. The high linearity, low variability, recoveries close to 100%, and sufficiently low LOD and LOQ values demonstrated that the developed UV-visible spectrophotometric method provided suitable analytical performance for the quantitative determination of CA in the NPs. The principal validation parameters are summarized in Table 1.

Table 1. Validation parameters of the UV-visible spectrophotometric method for CA in methanol:water (3:2, *v*/*v*) at 278 nm.

Validation Parameter	Result
Analytical wavelength	278 nm
Linearity range	2.5–17.5 µg/mL
Regression equation	y = 0.0385x + 0.0424
R^2	0.9993
LOD	0.4 µg/mL
LOQ	1.3 µg/mL
Precision levels	7.5, 10.0, 12.5 µg/mL
Precision (%RSD)	0.2–1.4%
Individual recovery	99.0–101.2%
Mean recovery at 7.5 µg/mL	99.4%
Mean recovery at 10.0 µg/mL	99.7%
Mean recovery at 12.5 µg/mL	100.2%
Accuracy (%RSD)	0.5–0.9%

2.2. Particle Size, Polydispersity Index, and Zeta Potential

The NPs were prepared using ERS 100 and/or ERL 100 as polymeric carriers. NP-1 and NP-4 contained ERS 100, NP-2 and NP-5 contained ERL 100, and NP-3 and NP-6 contained a 1:1 (*w*/*w*) ERS 100/ERL 100 blend. NP-1–NP-3 were prepared at a drug-to-polymer ratio of 1:1 (*w*/*w*), whereas NP-4–NP-6 were prepared at 1:2 (*w*/*w*). Blank-1, Blank-2, and Blank-3 were the corresponding drug-free NPs containing ERS 100, ERL 100, and their mixture, respectively (Table 2). In this study, NPs refer to submicron (<1 µm) solid polymeric colloidal carriers, consistent with terminology used in pharmaceutical drug delivery and studies employing the Nano Spray Dryer B-90 [17].

The PS, PDI, and ZP values are presented in Table 2. CA loading increased the mean PS from 340.9–359.5 nm for the blank NPs to 461.1–612.5 nm for the drug-loaded NPs. Relative to the corresponding blanks, PS increased by 67.6–70.4% for the 1:1 NPs and 35.3–40.1% for the 1:2 NPs. All 1:1 NPs were significantly larger than the 1:2 NPs ($p < 0.001$). The effect of polymer composition was comparatively small: only the ERS 100- and ERL 100-based NPs differed significantly at each drug-to-polymer ratio (NP-1 vs. NP-2 and NP-4 vs. NP-5; $p < 0.05$), while the blends showed intermediate values without significant differences from either single-polymer formulation. PDI values increased from 0.292–0.311 for the blank NPs to 0.351–0.467 after drug loading and were higher for the 1:1 NPs than for the 1:2 NPs.

All NPs exhibited positive ZP values (+36.8 to +43.6 mV). Drug-loaded NPs did not differ significantly from their corresponding blanks ($p > 0.05$). However, ERL 100-based NPs exhibited higher ZP values than the corresponding ERS 100-based NPs (Blank-2 vs. Blank-1, NP-2 vs. NP-1, and NP-5 vs. NP-4; $p < 0.01$), whereas the blends did not differ significantly from either single-polymer formulation.

Table 2. PS, PDI, and ZP of blank and CA loaded NPs.

NP Code	Particle Size (nm)	PDI	Zeta Potential (mV)
Blank-1	359.5 ± 18.5	0.311 ± 0.031	+39.4 ± 1.8
Blank-2	340.9 ± 16.7	0.292 ± 0.032	+43.6 ± 2.0
Blank-3	348.5 ± 17.6	0.309 ± 0.035	+41.5 ± 1.9
NP-1	612.5 ± 26.6	0.467 ± 0.046	+36.8 ± 2.3
NP-2	571.5 ± 21.6	0.424 ± 0.043	+41.7 ± 2.1
NP-3	591.8 ± 23.8	0.446 ± 0.048	+39.2 ± 2.2
NP-4	503.6 ± 24.6	0.389 ± 0.033	+37.6 ± 1.8
NP-5	461.1 ± 20.3	0.351 ± 0.039	+42.3 ± 1.9
NP-6	483.5 ± 21.3	0.360 ± 0.031	+40.1 ± 2.0

The increase in PS after CA loading may be explained by the higher total solids concentration of the spray-drying feed. Although the polymer concentration remained constant at 1 g/100 mL, adding CA increased the total solids concentration from 1% (w/v) for the blanks to 1.5% and 2% (w/v) for the 1:2 and 1:1 NPs, respectively. This is consistent with the observed PS order of blank < 1:2 < 1:1. Under otherwise comparable conditions, dry particle diameter increases approximately with the cube root of feed solids concentration. The observed PS increases exceeded those predicted from solids concentration alone, suggesting that other feed properties, including viscosity, may also have contributed; however, these properties were not measured. Differences in feed properties may likewise explain the smaller PS of ERL 100-based NPs compared with ERS 100-based NPs. The higher PDI values after CA loading indicate a broader particle-size distribution. The positive ZP values are consistent with the quaternary ammonium groups of both polymers and suggest a contribution from electrostatic stabilization under the measurement conditions. Nevertheless, measurements in distilled water do not establish long-term colloidal stability or predict dispersion behavior in physiological buffers or culture media [18,21,42–46].

2.3. Drug Content and Recovery of Cefuroxime Axetil

The theoretical drug content (DC) experimentally determined DC, and drug incorporation efficiency (DIE) of the prepared NPs are presented in Table 3. Because nano spray drying converts a single-phase feed into dry NPs without an external liquid phase, no unincorporated drug fraction remains in a continuous phase that could be separated by centrifugation. DC was therefore determined directly by dissolving a known mass of NPs, and the DIE was calculated as the ratio of the experimentally determined DC to the theoretical DC expected from the feed composition (×100). CA was not detected in the blank NPs. The experimental DC was 44.5–46.3% (w/w) for the 1:1 NPs and 30.6–31.7% (w/w) for the 1:2 NPs, close to the theoretical values of 50.0% and 33.3%, respectively. The DIE ranged from 89.0 ± 3.2% (NP-1) to 95.1 ± 2.4% (NP-5); at both drug-to-polymer ratios, the ERL 100-based NPs showed the highest and the ERS 100-based NPs the lowest values.

DIE, drug incorporation efficiency = (experimental DC/theoretical DC) × 100, where the theoretical DC is the drug fraction of the total solids in the feed [11,13,36,47]. Because the 1:1 and 1:2 NPs had different theoretical DCs, the DIE provides a more meaningful basis for comparison than the DC itself. The high values (89.0–95.1%) indicate that most of the CA in the feed was retained in the NPs, which can be attributed to the rapid solvent removal

and single-step particle formation of nano spray drying. The differences between polymer compositions were small, suggesting a limited influence of polymer composition on drug incorporation. Because CA was added to the feed before spray drying, the thermal exposure during processing should also be considered. Although the inlet temperature was 100 °C, the droplets remain close to the wet-bulb temperature of the solvent during evaporation, and the dried particles are exposed at most to the outlet temperature (54 ± 2 °C) for a residence time of only a few seconds before electrostatic collection. Consistent with this, the drug incorporation efficiency values were high, and the ^{1}H-NMR and FT-IR spectra (Sections 2.4 and 2.5) showed no signals or bands indicative of degradation. These results also suggest that subsequent differences in antibacterial and antibiofilm activity are unlikely to be explained solely by variations in DC, but may also reflect differences in polymer composition, surface properties, and NP-microorganism interactions.

Table 3. DC and DIE of CA in the prepared NPs.

NP Code	Theoretical DC (% *w*/*w*)	Experimental DC (% *w*/*w*)	DIE (%)
Blank-1	0	Not detected	-
Blank-2	0	Not detected	-
Blank-3	0	Not detected	-
NP-1	50.0	44.5 ± 1.6	89.0 ± 3.2
NP-2	50.0	46.3 ± 1.7	92.6 ± 3.4
NP-3	50.0	45.9 ± 1.8	91.8 ± 3.6
NP-4	33.3	30.6 ± 1.2	91.8 ± 3.6
NP-5	33.3	31.7 ± 0.8	95.1 ± 2.4
NP-6	33.3	31.5 ± 1.0	94.5 ± 3.0

2.4. ^{1}H-NMR Analysis

The ^{1}H-NMR spectra of the polymers, CA, and the blank and drug-loaded NPs are shown in Figure 1, and the principal signal assignments are summarized in Table 4. ERL 100 and ERS 100 showed comparable spectra, with aliphatic CH_3/CH_2 signals at δ 0.8–2.0 ppm and ester-associated signals at δ 3.4–4.2 ppm (Figure 1a,b). CA showed characteristic signals at δ 4.8–5.2, 5.9–6.1, and 6.9–7.6 ppm, which allowed it to be distinguished from the polymers (Figure 1c). The spectra of Blank-1-Blank-3 contained only polymer signals (Figure 1d–f), whereas those of NP-1–NP-6 contained the signals of both the polymer and CA, including the aromatic/furyl signals at δ 6.9–7.6 ppm (Figure 1g–l). No marked chemical-shift displacement or additional signals were observed among the drug-loaded NPs.

Table 4. Characteristic^{1}H-NMR chemical shifts and proton assignments of CA and Eudragit® polymers.

Chemical Shift (δ, ppm)	Proton Assignment	Main Component
0.8–2.0	Aliphatic CH_3 and CH_2 protons	ERS 100/ERL 100
3.4–4.2	Ester-associated O-CH_3 and O-CH_2 protons	ERS 100/ERL 100; overlapping drug signals
4.8–5.2	β-Lactam/oxymethine-associated protons	CA
5.9–6.1	Vinylic proton	CA
6.9–7.6	Aromatic/furyl-associated protons	CA

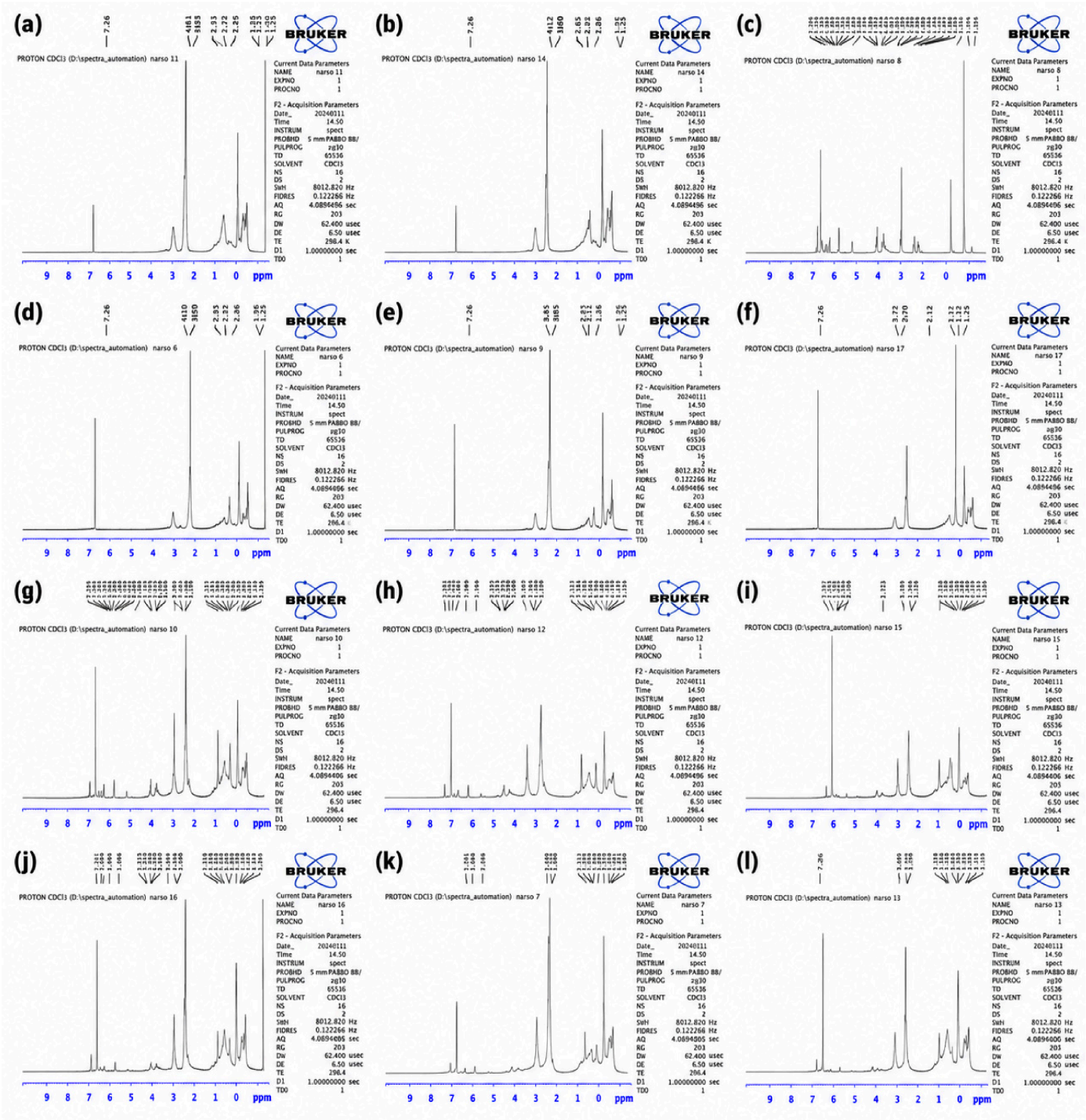


Figure 1. ^{1}H-NMR spectra of (**a**) ERL 100, (**b**) ERS100, (**c**) CA, (**d**) Blank-1, (**e**) Blank-2, (**f**) Blank-3, (**g**) NP-1, (**h**) NP-2, (**i**) NP-3, (**j**) NP-4, (**k**) NP-5, and (**l**) NP-6.

The ^{1}H-NMR spectra of ERL 100 and ERS 100 showed the expected aliphatic signals at approximately δ 0.8–2.0 ppm and methoxy/methylene signals associated with ester groups at δ 3.4–4.2 ppm, with highly similar profiles due to their common methacrylate backbone. Pure CA exhibited its characteristic aromatic signals at δ 6.9–7.6 ppm, together with β-lactam/oxymethine and aliphatic proton signals in the expected regions. Blank NPs displayed only polymer-related signals, whereas all drug-loaded NPs showed characteristic signals of both CA and the corresponding Eudragit® matrix. Importantly, the aromatic signals of CA remained detectable in all loaded NPs, confirming successful drug incorporation and preservation of its chemical structure after nano spray drying. No new signals or

major chemical shifts were observed, indicating the absence of detectable degradation or new covalent bond formation. Minor changes in chemical shift and signal intensity were attributed to physical interactions and changes in the local microenvironment within the polymer matrix. The relatively lower drug-signal intensity observed in the 1:2 drug NPs were consistent with their lower DC and higher polymer proportion [29,48–50].

2.5. Fourier Transform Infrared Spectroscopy (FT-IR) Analysis

The FT-IR spectra are shown in Figure 2, and the principal absorption bands are summarized in Table 5. ERL 100 and ERS 100 showed aliphatic C-H stretching bands at approximately 2900–2990 cm^{-1}, an ester carbonyl band at approximately 1726–1730 cm^{-1}, and ester C-O-C/C-O bands in the1065–1240cm^{-1} region (Figure 2a,b). CA showed characteristic bands at approximately 2939 and 2828 cm^{-1} and in the fingerprint region (1373, 1329, 1207, 1155, 1011, 939, and 756 cm^{-1}) (Figure 2c). The blank NPs retained the bands of their respective polymers without new bands (Figure 2d–f). In NP-1–NP-6, the polymer carbonyl band at approximately 1730 cm^{-1} was retained together with an additional carbonyl band at approximately 1788 cm^{-1} attributable to CA, and the characteristic bands of both components were preserved with only minor shifts in position and intensity (Figure 2g–l). No bands attributable to newly formed functional groups were detected. These findings were consistent with the ^{1}H-NMR results and supported the incorporation of CA into the Eudragit® polymer matrix of the NPs without evidence of new covalent bond formation [51–54].

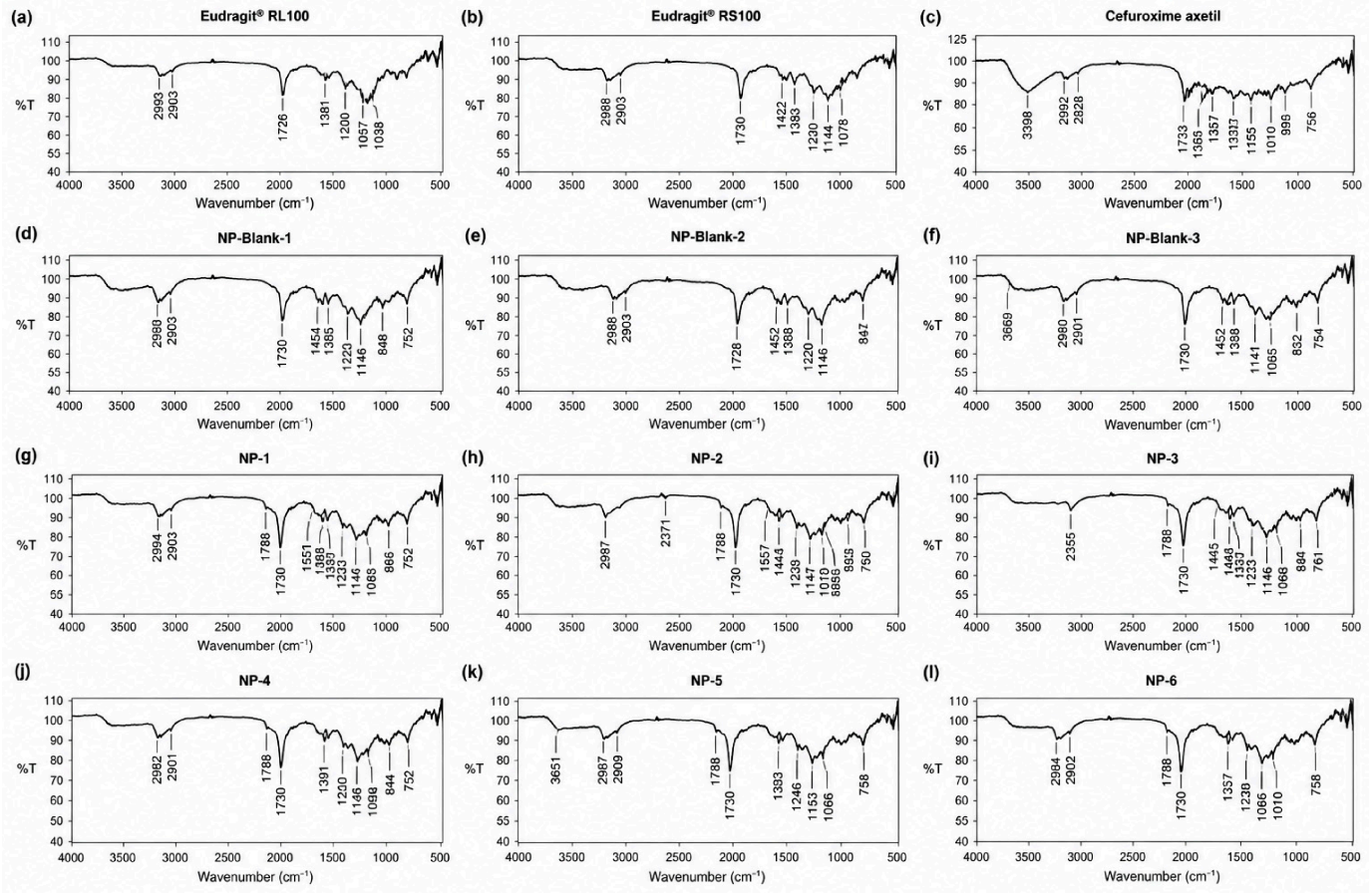


Figure 2. FT-IR spectra of (**a**) ERL 100, (**b**) ERS 100, (**c**) CA, (**d**) Blank−1, (**e**) Blank−2, (**f**) Blank−3, (**g**) NP−1, (**h**) NP−2, (**i**) NP−3, (**j**) NP−4, (**k**) NP−5, and (**l**) NP−6.

Table 5. Principal FT-IR absorption bands identified in the raw materials and NPs.

Wavenumber (cm^{-1})	Assignment	Eudragit® Polymers/Blank NPs	Drug-Loaded NPs
2900–2990	Aliphatic C-H stretching	✓	✓
~1788	CA associated carbonyl band	-	✓
~1730	Ester carbonyl (C=O)	✓	✓
1330–1380	CH_3 deformation region	✓	✓
~1240	Ester C-O-C stretching	✓	✓
1145–1155	Ester C-O stretching	✓	✓
1010–1065	C-O stretching region	✓	✓
756–939	Characteristic fingerprint region of cefuroxime axetil	-	✓

Table note: ✓ indicates the presence of the specified property or activity; - indicates its absence.

The physicochemical findings provide an important basis for interpreting the microbiological results. The PS, PDI, ZP, DC, and DIE data demonstrated that nano spray drying generated particulate systems whose properties varied according to polymer composition. Furthermore, FT-IR and ^{1}H-NMR analyses supported the structural preservation of CA after formulation. In particular, the characteristic CA signals remained detectable in drug-loaded NPs without the appearance of new signals indicative of major covalent modification. These observations are relevant microbiologically because they support the interpretation that the antibacterial effects observed after nano spray drying originated from retained CA rather than from a newly formed chemical derivative.

2.6. Antibacterial Activity of CA Loaded NPs

The antibacterial activity of CA loaded Eudragit® NPs was evaluated against *Bacillus subtilis* NRRL B478, *Staphylococcus aureus* ATCC 29213, and *Escherichia coli* ATCC 25922 using agar well diffusion and broth microdilution assays. All CA-loaded NPs exhibited detectable antibacterial activity, whereas blank NPs showed no inhibition under the tested conditions (Figures 3 and 4; Table 6).

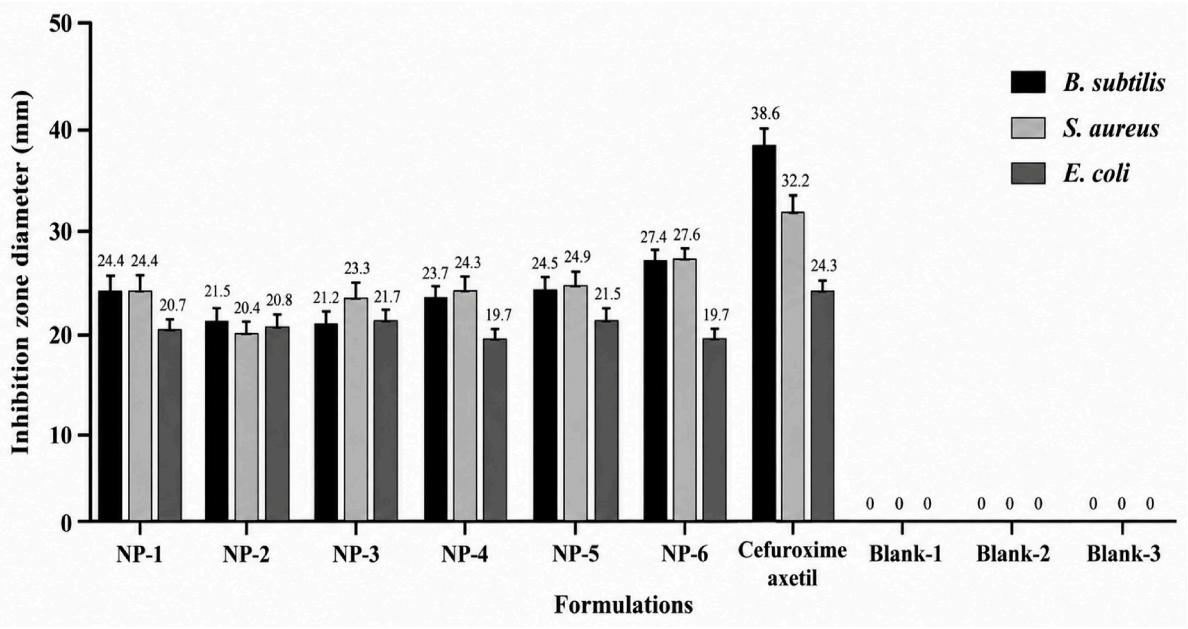


Figure 3. Antibacterial activity of CA loaded NPs, free CA, and blank NPs (Blank-1, Blank-2 and Blank-3). Inhibition zone diameters are expressed in mm and presented as mean ± SD from three independent experiments.

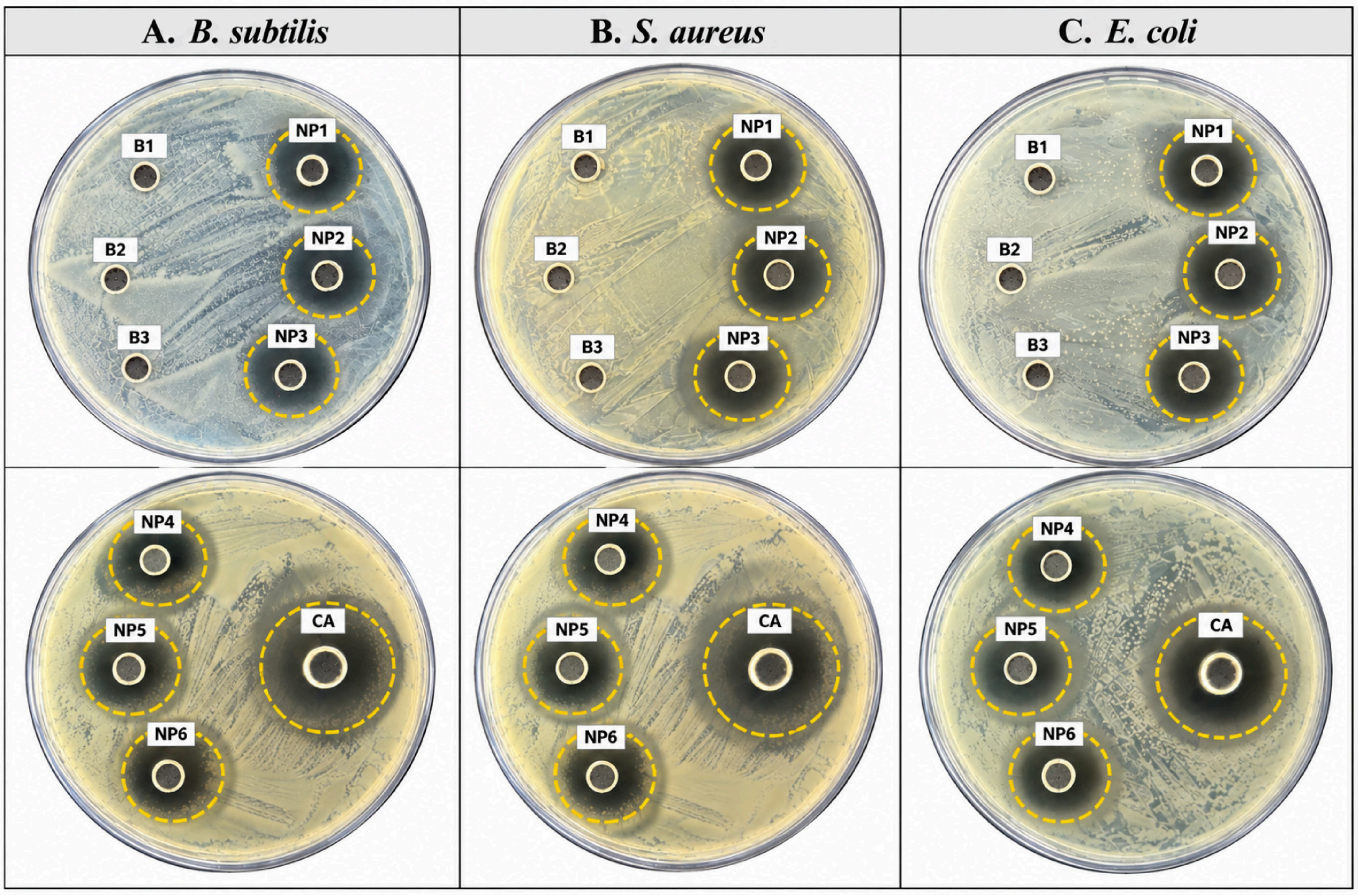


Figure 4. Representative agar well diffusion photographs showing inhibition zones against (**A**) *B. subtilis*, (**B**) *S. aureus*, and (**C**) *E. coli*. NP-1–NP-6: CA loaded NPs; B1–B3: blank NPs; CA: free cefuroxime axetil. Yellow dashed circles indicate inhibition zones.

Table 6. Minimum inhibitory concentration (MIC) (μg/mL) values of CA loaded NPs, free CA, and blank NPs (Blank-1–Blank-3).

	B. subtilis	*S. aureus*	*E. coli*
NP-1	62.5	31.25	31.25
NP-2	125	500	62.5
NP-3	250	500	125
NP-4	125	250	62.5
NP-5	62.5	250	62.5
NP-6	250	250	125
CA	2	4	8
Blank-1	-	-	-
Blank-2	-	-	-
Blank-3	-	-	-

In the agar well diffusion assay, NP-1–NP-6 produced inhibition zones of 21.2–27.4 mm against *B. subtilis*, 20.4–27.6 mm against *S. aureus*, and 19.7–21.7 mm against *E. coli*. NP-6 produced the largest zones against *B. subtilis* (27.4 mm) and *S. aureus* (27.6 mm), whereas NP-3 produced the largest zone against *E. coli* (21.7 mm). Free CA exhibited larger inhibition zones of 38.6, 32.2, and 24.3 mm, respectively. These findings confirm that CA-loaded NPs retained measurable antibacterial activity after NP preparation, although none exceeded free CA in agar diffusion.

The absence of detectable inhibition by blank NPs suggests that the observed agar diffusion activity was primarily associated with incorporated CA rather than the polymer carriers. Smaller inhibition zones for the NPs may reflect differences in drug availability and diffusion through the agar matrix, consistent with previous investigations of Eudragit®-based antibiotic delivery systems. However, this mechanism cannot be confirmed without direct drug-release measurements. Differences among bacterial species may also reflect strain-specific susceptibility and cell-envelope characteristics rather than a generalized preference for Gram-positive bacteria.

The MIC results showed a different NP-dependent pattern. NP-1 exhibited the lowest overall MIC values among the NPs (62.5 µg/mL against *B. subtilis* and 31.25 µg/mL against both *S. aureus* and *E. coli*), although NP-5 showed an identical MIC against *B. subtilis*. In contrast, NP-6, which produced the largest inhibition zones against the Gram-positive strains, exhibited MIC values of 250 µg/mL against both organisms. Free CA showed lower nominal MIC values of 2, 4, and 8 µg/mL against *B. subtilis*, *S. aureus*, and *E. coli*, respectively. However, direct potency comparisons are limited because NP concentrations represent total NP mass rather than equivalent amounts of CA. The differences between agar diffusion and MIC results highlight the distinct endpoints of these assays. Agar diffusion depends partly on the migration of antibacterial compounds through a solid medium, whereas broth microdilution measures growth inhibition in liquid culture [55]. Polymer composition, particle dispersion, and drug availability may contribute to the observed NP-dependent differences [56]. Although incorporation into Eudragit® matrices could modify CA availability, controlled release or prolonged antibacterial activity cannot be established from the present assays alone. Therefore, the principal finding is the retention of measurable antibacterial activity after nanoencapsulation, with differences among NPs that warrant further investigation using drug-release and pharmacologically normalized comparative studies.

Drug-Content-Normalized Antibacterial Activity

To enable a more meaningful comparison between free CA and CA-loaded Eudragit® NPs, the experimentally determined minimum inhibitory concentration (MIC) values were normalized according to the drug content of each NP (Table 7). The calculated CA-equivalent MIC values ranged from 19.81 to 114.75 µg/mL against *Bacillus subtilis*, 13.91 to 231.50 µg/mL against *Staphylococcus aureus*, and 13.91 to 57.38 µg/mL against *Escherichia coli*. Relative to free CA, the corresponding MIC fold-change values ranged from 9.91 to 57.38, 3.48 to 57.88, and 1.74 to 7.17, respectively.

Table 7. Drug-content-normalized MIC values and fold-change relative to free CA.

NP Code	DC (%)	*B. subtilis* CA-eq MIC	Fold	*S. aureus* CA-eq MIC	Fold	*E. coli* CA-eq MIC	Fold
NP-1	44.5	27.81	13.91	13.91	3.48	13.91	1.74
NP-2	46.3	57.88	28.94	231.50	57.88	28.94	3.62
NP-3	45.9	114.75	57.38	229.50	57.38	57.38	7.17
NP-4	30.6	38.25	19.13	76.50	19.13	19.13	2.39
NP-5	31.7	19.81	9.91	79.25	19.81	19.81	2.48
NP-6	31.5	78.75	39.38	78.75	19.69	39.38	4.92
Free CA	100	2.00	1.00	4.00	1.00	8.00	1.00

Table note: DC, drug content; CA-eq MIC, nominal cefuroxime axetil-equivalent minimum inhibitory concentration (µg/mL). Fold-change was calculated by dividing CA-eq MIC by the corresponding MIC of free CA.

Among the NPs, NP-1 exhibited the lowest CA-equivalent MIC values against *S. aureus* and *E. coli* (13.91 µg/mL for both strains), whereas NP-5 demonstrated the lowest value against *B. subtilis* (19.81 µg/mL). However, all NPs exhibited higher CA-equivalent MIC

values than free CA, indicating that NP incorporation did not improve immediate planktonic antibacterial potency under the tested conditions.

The differences in inhibitory concentrations may be influenced by NP-dependent antibiotic availability, although this mechanism was not directly investigated. Importantly, the calculated CA-equivalent MIC values represent nominal incorporated drug concentrations rather than the amount of antibiotic released during incubation. Consequently, differences in antibacterial activity cannot be attributed to controlled release or polymer-mediated delivery without experimental release data. Standardized drug-release testing is essential for characterizing colloidal delivery systems and interpreting the relationship between NP composition and drug availability [57].

These findings clarify that the primary contribution of the developed NPs lies in the NP-dependent modification of physicochemical and microbiological characteristics rather than demonstrated superiority over free CA. Further investigations involving drug-release kinetics and drug-equivalent antibacterial comparisons are required to establish whether the polymeric carriers provide additional delivery-related benefits.

2.7. Time-Kill Kinetics

The time-dependent antibacterial activity of CA-loaded NPs (NP-1–NP-6) was evaluated against *Staphylococcus aureus* ATCC 29213 and *Escherichia coli* ATCC 25922 at 62.5, 125, and 250 μg/mL over 24 h (Figure 5). Viable bacterial counts were determined at 0, 2, 4, 6, 8, and 24 h. Across both strains, NP-treated groups generally exhibited lower bacterial counts than untreated growth controls, although the magnitude of growth suppression varied among NPs and concentrations.

For *S. aureus*, NP-treated bacterial counts remained approximately 6.7–7.1 $\log_{10}$ CFU/mL, compared with 7.7–8.1 $\log_{10}$ CFU/mL in untreated controls. At 250 and 125 μg/mL, the NPs showed broadly similar profiles, whereas greater variability occurred at 62.5 μg/mL. For *E. coli*, NP-treated counts generally ranged from 6.7 to 7.3 $\log_{10}$ CFU/mL, remaining below the corresponding growth controls throughout the observation period. Free CA consistently produced lower viable counts than the NPs. Importantly, none of the NPs achieved a $\geq$3 $\log_{10}$ CFU/mL reduction relative to the initial bacterial counts, indicating that the conventional criterion for bactericidal activity was not met. Thus, the observed effects are more appropriately described as suppression of bacterial proliferation relative to untreated controls rather than confirmed bacterial killing. These findings provide time-dependent information complementary to the MIC results but do not establish sustained drug release or superior antibacterial efficacy. The relationship between tested concentrations and NP-specific MIC values further limits direct comparisons. Against *S. aureus*, the concentrations corresponded to 2×–8× MIC for NP-1 but remained below the MICs of NP-2 and NP-3. For *E. coli*, the tested concentrations reached or exceeded the MICs of all NPs at one or more concentrations. Because NP concentrations were expressed as total NP mass rather than CA-equivalent concentrations, differences in drug content may also influence their apparent antibacterial performance. Moreover, the free-drug and NP groups were not compared on an equivalent active-drug basis. The time-kill results demonstrate NP-dependent growth suppression without confirmed bactericidal activity. Although Eudragit® incorporation may modify antibiotic availability, this potential advantage requires direct release studies and drug-equivalent comparisons before conclusions regarding prolonged antimicrobial activity or therapeutic benefit can be drawn.

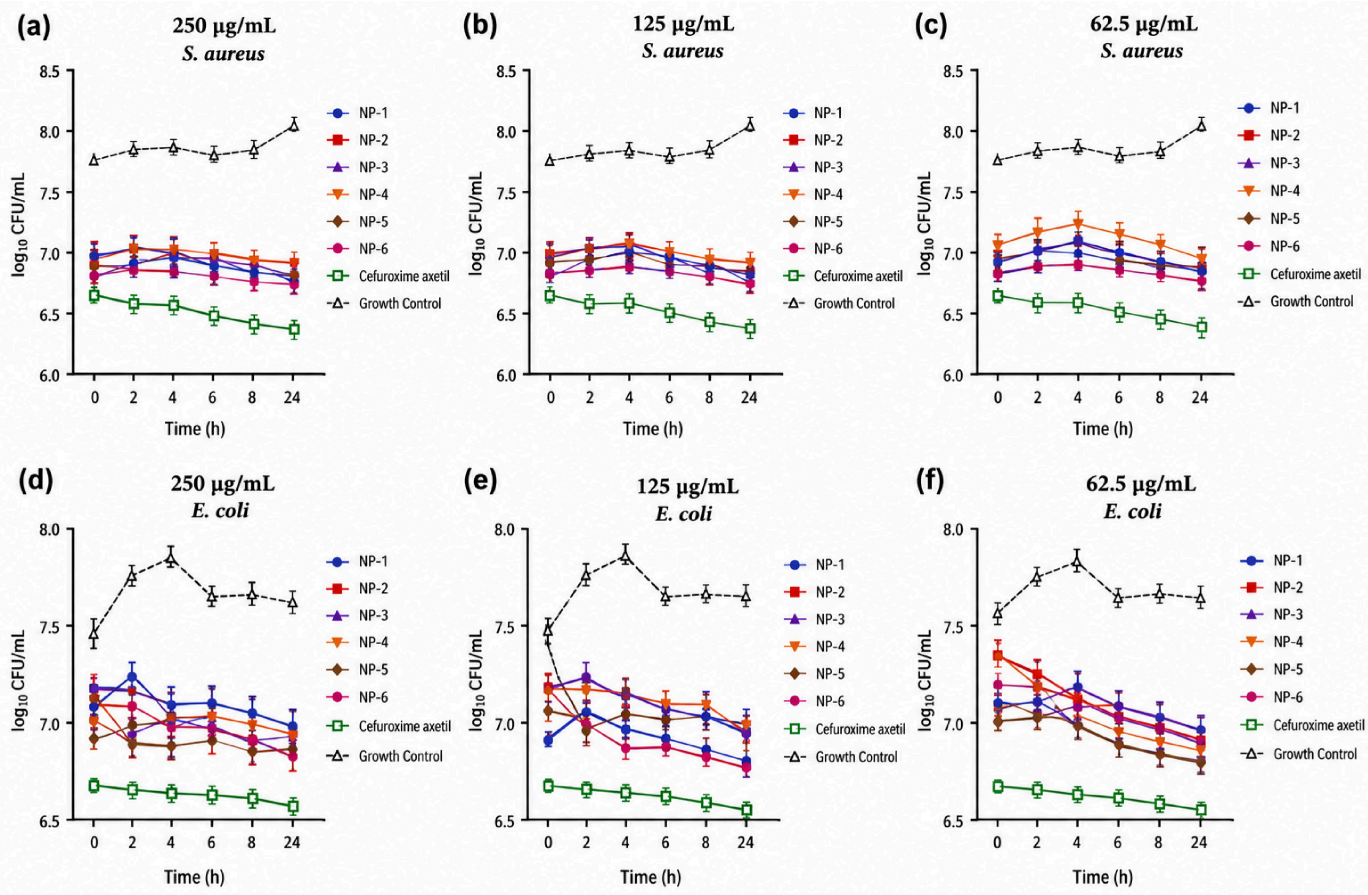


Figure 5. Time-kill profiles of cefuroxime axetil (CA)-loaded nanoparticles (NPs) and free CA against *Staphylococcus aureus* and *Escherichia coli* at different concentrations: (**a**) *S. aureus* at 250 µg/mL; (**b**) *S. aureus* at 125 µg/mL; (**c**) *S. aureus* at 62.5 µg/mL; (**d**) *E. coli* at 250 µg/mL; (**e**) *E. coli* at 125 µg/mL; and (**f**) *E. coli* at 62.5 µg/mL. Viable bacterial counts were determined at 0, 2, 4, 6, 8, and 24 h and expressed as $\log_{10}$ CFU/mL. The growth control represents untreated bacterial cultures. Data are presented as mean ± SD from three independent experiments. Concentrations of NP-1–NP-6 are expressed as nanoparticle concentrations (µg/mL).

MIC-Normalized Interpretation of Time-Kill Kinetics

To further characterize the time-dependent antibacterial responses, the concentrations used in the time-kill experiments were expressed as multiples of the NP-specific MIC values (Table 8). This analysis demonstrated considerable differences in relative antimicrobial exposure among NPs, despite the use of identical nominal concentrations of 62.5, 125, and 250 µg/mL.

To further characterize the time-dependent antibacterial responses, the concentrations used in the time-kill experiments were expressed as multiples of the NP-specific MIC values (Table 8). This analysis demonstrated considerable differences in relative antimicrobial exposure among NPs, despite the use of identical nominal concentrations of 62.5, 125, and 250 µg/mL. Against *S. aureus*, these concentrations corresponded to 2×, 4×, and 8× MIC for NP-1, respectively, whereas they represented only 0.125×, 0.25×, and 0.5× MIC for NP-2 and NP-3. For NP-4, NP-5, and NP-6, the exposure ratios ranged from 0.25× to 1× MIC. Against *E. coli*, NP-1 was evaluated at 2–8× MIC, NP-2, NP-4, and NP-5 at 1–4× MIC, and NP-3 and NP-6 at 0.5–2× MIC. These findings indicate that several NPs, particularly NP-2 and NP-3 against *S. aureus*, were evaluated predominantly at sub-MIC concentrations.

Table 8. MIC-normalized exposure ratios of CA-loaded NPs and free CA during time-kill experiments.

NP Code	*S. aureus* 62.5 µg/mL	*S. aureus* 125 µg/mL	*S. aureus* 250 µg/mL	*E. coli* 62.5 µg/mL	*E. coli* 125 µg/mL	*E. coli* 250 µg/mL
NP-1	2.00	4.00	8.00	2.00	4.00	8.00
NP-2	0.125	0.25	0.50	1.00	2.00	4.00
NP-3	0.125	0.25	0.50	0.50	1.00	2.00
NP-4	0.25	0.50	1.00	1.00	2.00	4.00
NP-5	0.25	0.50	1.00	1.00	2.00	4.00
NP-6	0.25	0.50	1.00	0.50	1.00	2.00
Free CA	15.625	31.25	62.50	7.8125	15.625	31.25

Table note: Values represent multiples of the corresponding NP-specific MIC (× MIC). Concentration headings are expressed in µg/mL. Ratios below 1 indicate sub-MIC exposure. For NP-NPs, concentrations refer to total NP mass; for free CA, concentrations refer to antibiotic mass. These ratios therefore characterize relative MIC exposure rather than equivalent delivered drug concentrations.

This distinction is important when interpreting the time-kill profiles. The relatively limited growth suppression observed with NP-2 and NP-3 against *S. aureus* may partly reflect their sub-MIC exposure conditions rather than differences in NP performance alone. In contrast, NP-1 was evaluated at concentrations exceeding its MIC, providing a more favorable exposure relationship for bacterial growth inhibition. Nevertheless, the time-kill experiments did not consistently demonstrate a $\geq$3 $\log_{10}$ CFU/mL reduction from the initial bacterial count, which is conventionally used to define bactericidal activity. Therefore, the observed effects are more appropriately described as time-dependent bacterial growth suppression rather than confirmed bactericidal activity.

Furthermore, the tested concentrations of free CA corresponded to 15.625–62.5× MIC against *S. aureus* and 7.8125–31.25× MIC against *E. coli*, substantially exceeding the relative exposure levels of most NPs. Accordingly, the stronger antibacterial responses observed with free CA should be interpreted in the context of these differences in MIC-normalized exposure. The present findings support NP-dependent variation in antibacterial performance but do not demonstrate enhanced bactericidal activity or prolonged antibiotic release from the NP systems. Future studies conducted at matched MIC multiples and equivalent CA concentrations would provide a more rigorous assessment of the influence of Eudragit® composition on time-dependent antibacterial activity.

2.8. Antibiofilm Activity

The effects of CA-loaded NPs (NP-1–NP-6) on pre-established *Staphylococcus aureus* ATCC 29213 and *Escherichia coli* ATCC 25922 biofilms were evaluated using the crystal violet assay at concentrations of 15.62–500 µg/mL (Figure 6). All NPs reduced retained biofilm biomass in a concentration-dependent manner, whereas blank NPs showed no detectable effect under the tested conditions.

At 500 µg/mL, NPs produced biomass reductions of 96–98% against *S. aureus* and 95–97% against *E. coli*. Even at 15.62 µg/mL, reductions remained approximately 74–78% and 72–75%, respectively. NP-6 exhibited the highest numerical reductions at 500 µg/mL (98% against *S. aureus* and 97% against *E. coli*). Free CA produced comparable responses, ranging from 81% to 96% against *S. aureus* and 74% to 96% against *E. coli*. Thus, although some NPs showed numerically greater biomass reductions at selected concentrations, consistent superiority over free CA was not demonstrated.

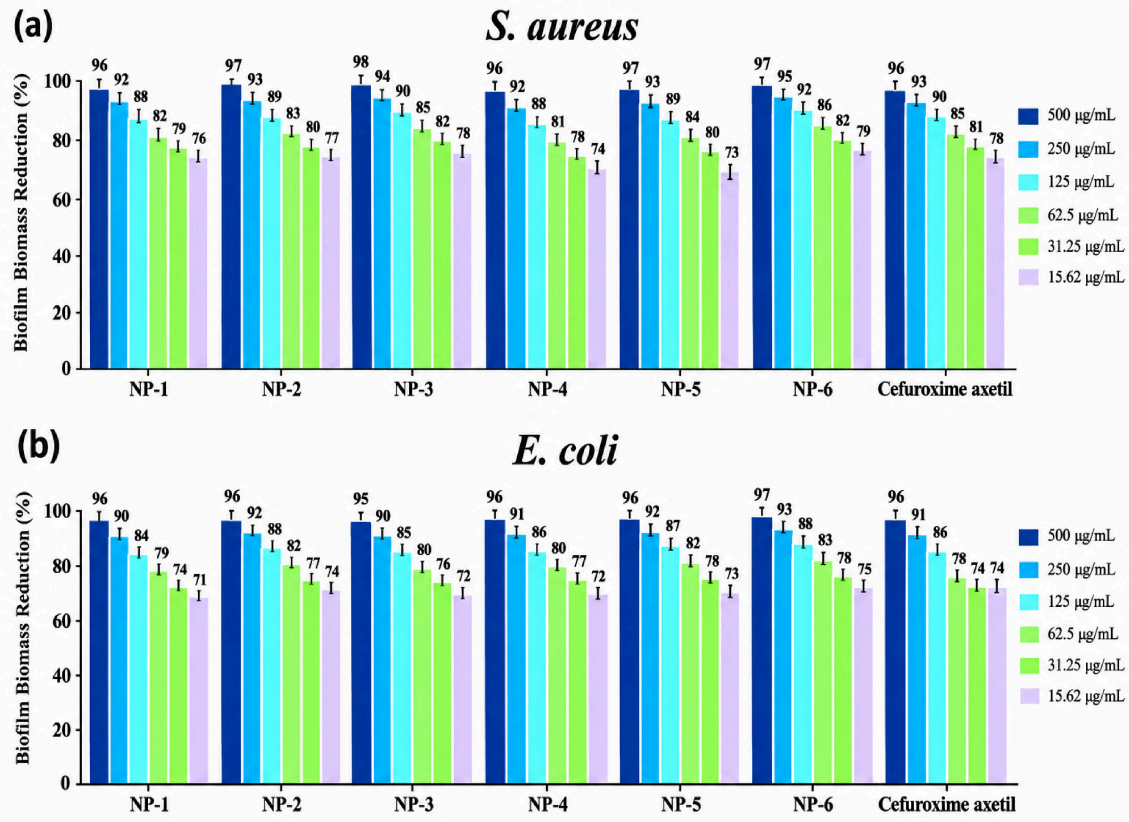


Figure 6. Biofilm biomass reduction (%) by CA loaded NPs (NP-1–NP-6) and free CA against pre-established biofilms of (**a**) *Staphylococcus aureus* ATCC 29213 and (**b**) *Escherichia coli* ATCC 25922 at concentrations ranging from 15.62 to 500 µg/mL. Bars represent mean values, and error bars indicate standard deviations (SD). Percentage values above the bars are rounded to the nearest whole number. Concentrations of NP-1–NP-6 are expressed as NP concentration (µg/mL).

Biofilm-associated antimicrobial tolerance involves extracellular matrix components, physiological heterogeneity, and persister populations [58–60]. Although the NPs produced substantial biomass reductions, these findings should be interpreted according to the limitations of crystal violet staining, which measures retained biomass rather than bacterial viability [61]. Consequently, the results do not establish bacterial killing, enhanced NP penetration, or complete biofilm eradication. Additional viability-based methods, such as biofilm CFU enumeration or metabolic assays, are required to validate these outcomes [62]. The discrepancy between planktonic MIC and biofilm biomass results was particularly evident for NP-2, which exhibited an MIC of 500 µg/mL against *S. aureus* but reduced retained biomass by approximately 97% at 500 µg/mL. This difference reflects the distinct experimental endpoints rather than evidence of enhanced antibiofilm potency. Similarly, NP-6 showed favorable numerical performance in agar diffusion and biomass reduction assays but was not consistently superior across all microbiological tests.

Polymer composition may influence NP properties because ERL 100 exhibits greater aqueous permeability than ERS 100 [11] and previous studies have reported polymer-dependent differences in drug-delivery characteristics [63]. Particle size and surface properties may also affect interactions with biofilm matrices. However, drug release, NP penetration, and biofilm-associated bacterial viability were not directly assessed. Furthermore, washing-related variability and biofilm heterogeneity may influence crystal violet measurements [55,64,65]. Therefore, the present findings support the ability of CA-loaded NPs to reduce retained biofilm biomass under the tested conditions but do not demonstrate mechanistic or therapeutic superiority over free CA.

2.8.1. Integrated Concentration–Response Analysis of Antibiofilm Activity

To provide an integrated quantitative assessment of antibiofilm performance, the area under the concentration–response curve (AUC) was calculated using the percentage reduction in pre-established biofilm biomass across six concentrations (15.62–500 µg/mL). This analysis enabled comparison of the overall concentration-dependent responses of all six NPs and free CA, rather than relying exclusively on individual concentration points. Against *S. aureus*, NP-6 exhibited the highest AUC (133.37), followed by NP-3 (132.16), free CA (131.26), NP-2 (130.06), NP-5 (129.75), NP-1 (128.55), and NP-4 (127.65). Similarly, NP-6 demonstrated the highest AUC against *E. coli* (128.85), followed by NP-5 (127.50), NP-2 (127.05), NP-4 (125.84), NP-3 (124.79), free CA (124.64), and NP-1 (123.58) (Table 9).

Table 9. Concentration–response area under the curve (AUC) values for biofilm biomass reduction.

NP Code	*S. aureus* AUC	*E. coli* AUC
NP-1	128.55	123.58
NP-2	130.06	127.05
NP-3	132.16	124.79
NP-4	127.65	125.84
NP-5	129.75	127.50
NP-6	133.37	128.85
Free CA	131.26	124.64

Table note: AUC values were calculated using the trapezoidal rule from the six biofilm biomass reduction percentages shown in the experimental figure, across $\log_{10}$-transformed concentrations of 15.62–500 µg/mL. Higher AUC values indicate greater integrated biofilm biomass reduction over the investigated concentration range.

These findings indicate that NP-6 exhibited the highest numerical AUC values against both bacterial species, reflecting the greatest integrated reduction in retained biofilm biomass across the tested concentration range. However, the differences between NPs were relatively small, particularly against *S. aureus*, and should be interpreted descriptively because replicate-level statistical comparisons were not performed. Furthermore, the crystal violet assay measures retained biofilm biomass rather than bacterial viability [61]. Therefore, the AUC results provide a complementary quantitative assessment of concentration-dependent antibiofilm responses but do not establish statistically significant differences, bacterial killing, or complete biofilm eradication.

2.8.2. Integrated Interpretation of Antibacterial and Antibiofilm Performance

The additional quantitative analyses provide a more comprehensive interpretation of the microbiological performance of CA-loaded Eudragit® NPs. Drug-content-normalized MIC calculations demonstrated that free CA retained greater immediate inhibitory activity against planktonic bacteria, while NP-1 exhibited the most favorable CA-equivalent MIC profile against *S. aureus* and E. coli among the NPs. MIC-normalized time-kill analysis further revealed that several NPs were evaluated at sub-MICs, emphasizing the importance of considering relative antimicrobial exposure when interpreting time-dependent responses. In contrast, concentration–response analysis of pre-established biofilms demonstrated substantial biomass reduction across the evaluated NPs, with NP-6 exhibiting the highest numerical AUC values against both *S. aureus* and *E. coli*. However, these descriptive differences do not establish statistical superiority, and the crystal violet assay does not directly measure bacterial viability [61].

Comparison of NPs prepared with the same polymer composition further revealed that increasing the polymer proportion from a drug-to-polymer ratio of 1:1 to 1:2 did not consistently improve antibacterial activity. Among ERS100-based NPs, NP-1 exhibited lower MIC values than NP-4, whereas increasing the polymer proportion in ERL100-based NPs

(NP-2 versus NP-5) and ERS 100/RL 100-based NPs (NP-3 versus NP-6) resulted in lower MIC values against *S. aureus*. These findings indicate that the relationship between polymer proportion and antibacterial performance varies according to polymer composition and bacterial species. Moreover, the differences between NP-1, which demonstrated the most favorable overall planktonic MIC profile, and NP-6, which exhibited the highest numerical antibiofilm AUC values, suggest that stronger planktonic antibacterial activity does not necessarily correspond to greater reduction in established biofilm biomass. Although variations in polymer permeability, drug incorporation, particle characteristics, and drug availability may contribute to these observations, their individual contributions cannot be established from the present findings.

Collectively, these results indicate that neither polymer composition nor drug-to-polymer ratio alone reliably microbiological performance. The principal contribution of the developed NPs is therefore the demonstration of NP-dependent physicochemical and microbiological characteristics rather than improved intrinsic antibacterial potency. Furthermore, the antibiofilm comparisons were performed at equal nominal NP concentrations rather than equivalent CA concentrations, limiting direct conclusions regarding the influence of nanoencapsulation on antibiofilm activity. Potential advantages related to controlled release, biofilm penetration, or therapeutic performance also remain unverified. Future investigations should therefore prioritize quantitative drug-release studies, drug-equivalent antibacterial and antibiofilm comparisons, biofilm-associated viable counts, and complementary physicochemical characterization to determine whether the observed NP-dependent differences translate into meaningful drug-delivery benefits.

3. Limitations and Future Perspectives

Several limitations should be acknowledged. The absence of direct drug-release studies and experimentally matched drug-equivalent comparisons limits conclusions regarding drug availability and relative antibacterial performance. Although drug-content- and MIC-normalized analyses provided additional insights, they cannot replace direct experimental comparisons. Antibiofilm activity was assessed using crystal violet staining, which measures biofilm biomass rather than bacterial viability, while AUC comparisons remained descriptive without replicate-level statistical analysis. Furthermore, physicochemical characterization lacked SEM/TEM imaging, surface-associated drug quantification, and stability-indicating chromatographic analysis. Microbiological experiments were restricted to reference strains under static in vitro conditions. Future studies should investigate drug-release kinetics, biofilm-associated bacterial viability, and NP stability, alongside drug-equivalent comparisons and clinically relevant biological models, to establish whether CA-loaded NPs provide meaningful advantages for antibiotic delivery.

4. Materials and Methods

4.1. Materials

Cefuroxime axetil (CA) was used as the active pharmaceutical ingredient and was kindly provided by SANOVEL Pharmaceutical Industry and Trade Inc. (Istanbul, Türkiye). Eudragit® RS100 (ERS100) and Eudragit® RL100 (ERL100) were generously supplied by Evonik GmbH (Darmstadt, Germany). Analytical-grade ethanol and methanol (Merck, Darmstadt, Germany) were used as organic solvents during nanoparticle (NP) preparation and analytical procedures, while ultrapure water was obtained using a Milli-Q® water purification system (Merck Millipore, Darmstadt, Germany). All solvents used for UV–visible spectrophotometric analyses were of analytical grade.

Mueller–Hinton agar (MHA) and Mueller–Hinton broth (MHB) were obtained from Merck (Darmstadt, Germany). MHA was used for agar well diffusion assays and viable

bacterial enumeration, whereas MHB was used for broth microdilution and antibiofilm assays. The bacterial strains investigated were *Bacillus subtilis* NRRL B-478, *Staphylococcus aureus* ATCC 29213, and *Escherichia coli* ATCC 25922. All culture media, chemicals, and microbiological consumables were of appropriate microbiological or analytical grade.

CA-loaded and blank polymeric NPs were prepared using a Nano Spray Dryer B-90 (BÜCHI Labortechnik AG, Flawil, Switzerland). Centrifugation was performed using an Eppendorf centrifuge (Eppendorf SE, Hamburg, Germany). Particle size, polydispersity index (PDI), and zeta potential were measured using a Zetasizer Nano ZS (Malvern Instruments Ltd., Worcestershire, UK). CA content was determined using a UV-1800 UV–visible spectrophotometer (Shimadzu, Kyoto, Japan). FT-IR analyses were performed using an IRPrestige-21 spectrophotometer (Shimadzu, Kyoto, Japan), whereas ^{1}H-NMR spectra were obtained using a Bruker NMR spectrometer (Bruker BioSpin GmbH & Co. KG, Rheinstetten, Germany).

4.2. UV-Visible Spectrophotometric Method and Validation

Quantitative determination of CA was performed using a UV-1800 UV–visible spectrophotometer (Shimadzu, Kyoto, Japan). The method was validated for linearity, precision, accuracy, and analytical sensitivity following the principles of ICH Q2(R2) [66–70] CA standard solutions were prepared in methanol: water (3:2, v/v), and absorbance was measured at 278 nm. Linearity was assessed using three independently prepared calibration curves over 2.5–17.5 µg/mL. Precision and accuracy were evaluated at 7.5, 10.0, and 12.5 µg/mL using independently prepared solutions analyzed in triplicate over three consecutive days. Intra- and interday precision were expressed as %RSD, and accuracy as percentage recovery relative to nominal concentrations. LOD and LOQ were calculated from the calibration data [71]. Following validation, the method was used for quantitative determination of CA in the NPs [72,73].

4.3. Preparation of CA- Loaded NPs

CA-loaded NPs were prepared using the nano spray-drying technique with a Nano Spray Dryer B-90 (BÜCHI Labortechnik AG, Flawil, Switzerland). Nano spray drying was selected because of its suitability to produce small dry particles from pharmaceutical NPs and its compatibility with organic solvent-based feed systems. ERS 100 and ERL 100 were selected as the polymeric carriers. The principal difference between the two polymers is their relative content of quaternary ammonium groups, with ERL 100 exhibiting greater permeability than ERS 100. These properties make the polymers suitable for modifying drug incorporation and transport through polymeric matrices.

To investigate the influence of polymer composition and drug-to-polymer ratio, six CA-loaded NPs were prepared using ERS 100 alone, ERL 100 alone, or a 1:1 combination of ERS 100 and ERL 100. Drug-to-polymer ratios of 1:1 and 1:2 were investigated. In addition, three drug-free NPs, Blank-1, Blank-2, and Blank-3, were prepared as corresponding controls. The use of blank NPs enabled assessment of whether the polymeric carriers themselves contributed to the observed biological effects [74]. The complete compositions of the NPs are presented in Table 10.

For each NP, the required amount of Eudragit® polymer was dissolved in 100 mL of ethanol and stirred magnetically at 250 rpm for approximately 30 min at room temperature until a clear polymer solution was obtained. CA was subsequently added at the amount specified for each NP, and stirring was continued for an additional 30 min to obtain a homogeneous feed solution. Blank NPs were prepared using the same procedure without the addition of CA. Because CA and the polymer were contained in the same feed and solidified together during solvent evaporation from each droplet, the resulting NPs are

matrix-type systems in which the drug is physically dispersed throughout the polymer; no surface functionalization or chemical conjugation was involved. Before processing the NPs, the Nano Spray Dryer B-90 was conditioned with ethanol for approximately 30 min. The prepared feed solutions were then processed using a vibrating mesh atomization system equipped with a 4 µm mesh membrane at an inlet temperature of 100 °C, resulting in an outlet temperature of 54 ± 2 °C. All NPs were produced under identical processing conditions to enable direct comparison between NPs. The operating parameters are summarized in Table 11. The preparation procedure and processing conditions were based on established applications of Nano Spray Dryer B-90 technology for pharmaceutical NP production.

Table 10. Composition of CA-loaded and blank NPs.

NP Code	Drug: Polymer Ratio	ERS 100	ERL 100	CA	Ethanol
Blank-1	-	1 g	-	-	100 mL
Blank-2	-	-	1 g	-	100 mL
Blank-3	-	0.5 g	0.5 g	-	100 mL
NP-1	1:1	1 g	-	1 g	100 mL
NP-2	1:1	-	1 g	1 g	100 mL
NP-3	1:1	0.5 g	0.5 g	1 g	100 mL
NP-4	1:2	1 g	-	0.5 g	100 mL
NP-5	1:2	-	1 g	0.5 g	100 mL
NP-6	1:2	0.5 g	0.5 g	0.5 g	100 mL

Table 11. Operating conditions used for nano spray drying of the NPs.

Parameter	Operating Condition
Instrument	Nano Spray Dryer B-90 (BÜCHI Labortechnik AG, Flawil, Switzerland)
Atomization system	Vibrating mesh
Mesh aperture	4 µm
Solvent	Ethanol
Feed solution volume	100 mL
Inlet temperature	100 °C
Outlet temperature	54 ± 2 °C
Pump level	3
Spray level	100%
Particle collection system	Electrostatic collector
Feed-solution preparation	250 rpm for 30 min for polymer dissolution + 30 min after drug addition
Instrument conditioning	30 min with ethanol

Following nano spray drying, the resulting NPs were deposited in the electrostatic particle collector and carefully recovered using the dedicated collection system. The NPs were thus obtained directly as dry powders and were used as collected, without lyophilization or any additional drying step; all masses reported in this study refer to the nano-spray-dried powder. The powders were transferred to tightly closed amber glass containers and stored at room temperature protected from light and moisture until further physicochemical, structural, and microbiological analyses.

4.4. Particle Size, Polydispersity Index, and Zeta Potential

The mean hydrodynamic PS and PDI of the CA-loaded NPs were determined by dynamic light scattering (DLS) using a Zetasizer Nano ZS (Malvern Instruments Ltd., Worcestershire, UK). Prior to measurement, NP samples were dispersed at an appropriate concentration in distilled water without the addition of buffer or electrolyte (low-ionic-

strength medium) and briefly vortexed to obtain homogeneous dispersions. Measurements were performed at 25.0 ± 0.5 °C. Measurements were performed in backscatter mode (173°), and the refractive index and viscosity of the dispersant (water) were set to 1.330 and 0.8872 mPa·s (25 °C), respectively. The mean PS was reported as the intensity-weighted z-average diameter obtained by cumulants analysis, which depends on the dispersant properties but not on the refractive index of the particle material. ZP was determined on the same aqueous dispersions using the same instrument according to the electrophoretic light scattering (ELS) principle using disposable folded capillary cells (DTS1070, Malvern Instruments Ltd., Worcestershire, UK). PS, PDI, and ZP measurements were performed using six samples ($n = 6$), and the results were expressed as mean ± standard deviation. Similar DLS and electrophoretic mobility approaches have been employed for physicochemical characterization of NPs [75–78].

4.5. Determination of CA Content

The CA content of the NPs was determined using the validated UV-visible spectrophotometric method described above. Approximately 5 mg of each NP was accurately weighed and dispersed in 1 mL of methanol:water (3:2, v/v). Samples were vortexed for 5 min to ensure complete dissolution of the NPs. The resulting solutions were passed through a 0.22 µm membrane filter and appropriately diluted before spectrophotometric analysis at 278 nm. CA concentrations were calculated and the results were expressed as percentage drug content (DC). Comparable approaches involving disruption or dissolution of the polymeric matrix of the NPs followed by quantitative determination of the incorporated drug have been used for NP drug-content analysis [67,79]. The drug incorporation efficiency (DIE) was calculated as follows: DIE (%) = (experimental DC/theoretical DC) × 100, where the theoretical DC (50.0% and 33.3% w/w for the 1:1 and 1:2 NPs, respectively) corresponds to the drug fraction of the total solids in the feed. Because nano spray drying does not involve an external liquid phase, indirect determination of unincorporated drug in a supernatant was not applicable.

4.6. Proton Nuclear Magnetic Resonance (^{1}H-NMR) Analysis

^{1}H-NMR analysis was performed to investigate the structural characteristics of CA after NP incorporation and to evaluate potential molecular interactions between the CA and the Eudragit® polymers. Appropriate amounts of pure CA, blank NPs, and drug-loaded NPs were dissolved in deuterated chloroform ($CDCl_3$). The spectra were recorded at room temperature using a high-resolution Bruker NMR spectrometer operating at 400 MHz (Bruker BioSpin GmbH, Rheinstetten, Germany), and chemical shifts were expressed as δ values in parts per million (ppm). Spectra of the drug-loaded NPs were compared with those of pure CA and the corresponding blank NPs. Characteristic proton signals, possible chemical-shift changes, peak retention, and the appearance of new signals were evaluated to investigate drug-polymer interactions and structural preservation following NP preparation. NMR-based comparison of pure compounds and drug-loaded NP systems has similarly been employed for structural characterization of NPs [80,81].

4.7. Fourier-Transform Infrared Spectroscopy

FT-IR spectroscopy was performed to evaluate the structural characteristics of CA and possible interactions between the drug and polymeric components following NP formation. Spectra of pure CA, the individual polymers, blank NPs, and CA-loaded NPs were recorded using an FT-IR spectrophotometer (IR Prestige-21, Shimadzu Corporation, Kyoto, Japan). Spectra were acquired over the wavenumber range of 4000–500 cm^{-1}. Characteristic functional-group absorption bands of the drug-loaded NPs were compared with those of

pure CA, ERS 100, ERL 100, and the corresponding blank NPs. The presence, retention, disappearance, or shift of characteristic absorption bands and the possible appearance of new bands were evaluated to assess structural preservation and potential drug-polymer interactions following nano spray drying. FT-IR comparison of the active compound, polymeric carrier, and final NP is an established approach for investigating compatibility and potential molecular interactions in NP systems [82,83].

4.8. Antibacterial Activity

The antibacterial activity of CA-loaded NPs was assessed using agar well diffusion, broth microdilution, and time-kill assays, with free CA and corresponding blank NPs included as comparators. All microbiological experiments were performed in triplicate.

4.8.1. Agar Well Diffusion Assay

Antibacterial activity was evaluated using the agar well diffusion method [84,85] against *Staphylococcus aureus* ATCC 29213, *Escherichia coli* ATCC 25922, and *Bacillus subtilis* NRRL B-478. Fresh bacterial suspensions were spread onto Mueller–Hinton agar (MHA) plates. Wells (6 mm diameter, approximately 4 mm depth) were filled with 50 µL of each NP (500 µg/mL; 25 µg NPs/well), free CA, or corresponding blank NPs. Chloramphenicol served as the positive reference control. Plates were maintained at 4 °C for 2 h to allow pre-diffusion, followed by incubation at 37 °C for 24 h. Inhibition zone diameters were measured in millimeters.

4.8.2. Minimum Inhibitory Concentration

Minimum inhibitory concentrations (MICs) were determined by broth microdilution in 96-well plates following CLSI recommendations (2024). The same bacterial strains were tested using two-fold serial dilutions of NP-1–NP-6 and free CA (0.4–500 µg/mL) in Mueller–Hinton broth (MHB). Bacterial suspensions were adjusted to 0.5 McFarland (approximately 10^8 CFU/mL), and 100 µL of each dilution was mixed with 100 µL of bacterial suspension. Chloramphenicol and uninoculated MHB served as positive antibacterial and negative controls, respectively. Following incubation at 37 °C for 24 h, 20 µL of 0.01% (w/v) resazurin was added, and plates were incubated for another 4 h. MIC was defined as the lowest concentration showing no detectable bacterial growth based on the resazurin color response.

4.8.3. Drug-Content-Normalized MIC and Fold-Change Analysis

To enable quantitative comparison of the antibacterial activity of free CA and CA-loaded Eudragit® NPs, the experimentally determined minimum inhibitory concentration (MIC) values were normalized according to the drug content of each NP. The analysis included six NPs and three bacterial strains: *Bacillus subtilis*, *Staphylococcus aureus*, and *Escherichia coli*. The drug-content-normalized MIC, expressed as the nominal CA-equivalent MIC ($MIC_{CA\text{-}eq}$), was calculated using Equation (1).

$$MIC_{CA\text{-}eq} = MIC_{NP} \times (DC/100) \quad (1)$$

where MIC_{NP} represents the experimentally determined MIC expressed as total NP mass (µg/mL), and DC represents the experimentally measured drug content (% *w*/*w*).

To quantify the relative inhibitory activity of each NP compared with free CA, the MI fold-change was calculated using Equation (2):

$$\text{MIC fold-change} = MIC_{CA\text{-}eq}/MIC_{\text{free CA}} \quad (2)$$

where MIC_{free} CA represents the MIC of free CA against the corresponding bacterial strain. A fold-change value of 1 indicates an equivalent nominal antibiotic concentration at the

MIC endpoint, whereas values greater than 1 indicate that a higher nominal CA-equivalent concentration was required for growth inhibition compared with free CA. All calculations were performed using the experimentally determined MIC endpoints and NP-specific drug content values. The calculated CA-equivalent MIC values represent the nominal amount of incorporated antibiotic and should not be interpreted as the concentration of CA released from the NPs during incubation. Accordingly, the analysis was used for drug-content normalization rather than as a direct measurement of antibiotic release or bioavailability.

4.8.4. Time-Kill Assay

Time-kill kinetics were evaluated against *S. aureus* ATCC 29213 and *E. coli* ATCC 25922 using NP-1–NP-6 and free CA at 62.5, 125, and 250 μg/mL. Standardized bacterial suspensions were exposed to the NPs, and samples were collected at 0, 2, 4, 6, 8, and 24 h. Samples were serially diluted and plated onto MHA, followed by incubation at 37 °C for 24 h. Viable colonies were enumerated and expressed as $\log_{10}$ CFU/mL. Untreated cultures served as growth controls. Bactericidal activity was evaluated using the conventional criterion of a ≥3 $\log_{10}$ CFU/mL reduction relative to the initial viable count [86]. Time-kill curves were constructed by plotting viable counts against exposure time.

4.8.5. MIC-Normalized Time-Kill Exposure Analysis

To provide a concentration-adjusted interpretation of the time-kill experiments, the tested concentrations of CA-loaded NPs and free CA were normalized to their respective minimum inhibitory concentration (MIC) values. The analysis was performed separately for *Staphylococcus aureus* and *Escherichia coli* at the three tested concentrations of 62.5, 125, and 250 μg/mL. The MIC-normalized exposure ratio was calculated using Equation (3):

$$\text{MIC-normalized exposure ratio} = C_{test/}\text{MIC} \quad (3)$$

where C_{test} represents the nominal concentration used in the time-kill assay (μg/mL), and MIC represents the experimentally determined MIC of the corresponding NP against the same bacterial strain. The calculated exposure ratios were expressed as multiples of MIC (×MIC). Ratios below 1 were classified as sub-MIC exposures, a ratio of 1 represented exposure at the MIC, and ratios greater than 1 represented supra-MIC exposures.

The analysis was conducted to determine whether differences in time-dependent bacterial responses could be interpreted in relation to the relative inhibitory concentrations of individual NPs. Because the MIC values of free CA were expressed in antibiotic mass, whereas those of NPs were expressed in total NP mass, the calculated ratios were used only to characterize NP-specific MIC exposure levels. Time-kill responses were interpreted according to established principles for determining antimicrobial bactericidal activity. A reduction of at least 3 $\log_{10}$ CFU/mL from the initial viable bacterial count was considered the conventional threshold for bactericidal activity, whereas smaller reductions were interpreted as growth suppression unless additional evidence supported a bactericidal effect.

4.9. Antibiofilm Activity

The effects of CA-loaded NPs on pre-established *S. aureus* ATCC 29213 and *E. coli* ATCC 25922 biofilms were evaluated using the crystal violet microtiter plate assay [87,88]. Bacterial suspensions adjusted to 0.5 McFarland (approximately 10^8 CFU/mL) were dispensed into 96-well plates (200 μL/well) and incubated statically at 37 °C for 24 h to establish biofilms. Planktonic cells were removed, and wells were gently washed with phosphate-buffered saline (PBS). Established biofilms were treated with NP-1–NP-6 or free CA at 15.62–500 μg/mL (two-fold serial dilutions) for 48 h at 37 °C. Untreated biofilms and corresponding blank NPs served as controls. Following treatment, wells were washed

with PBS, fixed with methanol, stained with 0.1% crystal violet, and washed to remove excess dye. Retained crystal violet was solubilized with ethanol, and absorbance was measured at 550 nm. Biofilm biomass reduction was calculated relative to untreated controls (Equation (4)):

$$\text{Biofilm biomass reduction } (\%) = [(OD_{control} - OD_{sample)/}OD_{control}] \times 100 \quad (4)$$

Because crystal violet quantifies retained surface-associated biomass rather than bacterial viability, the results were interpreted as biomass reduction, not bacterial killing or biofilm eradication [89,90].

Concentration–Response AUC Analysis of Biofilm Biomass Reduction

To quantitatively compare the overall antibiofilm responses of CA-loaded Eudragit® NPs, the area under the concentration–response curve (AUC) was calculated using the biofilm biomass reduction percentages obtained from the crystal violet assay. The analysis included NP-1–NP-6 and free CA against *Staphylococcus aureus* and *Escherichia coli*. The biofilm biomass reduction percentages obtained at six concentrations (15.62, 31.25, 62.5, 125, 250, and 500 µg/mL) were used for the analysis. Concentrations were transformed to base-10 logarithmic values, and the AUC was calculated using the linear trapezoidal rule according to Equation (5):

$$AUC = \Sigma\,[(Y_i + Y_{i+1})/2] \times [\log_{10}(C_{i+1}) - \log_{10}(C_i)] \quad (5)$$

where Y_i and Y_{i+1} represent the percentage reductions in biofilm biomass at two consecutive concentrations, and C_i and C_{i+1} represent the corresponding concentrations (µg/mL). The summation was performed across the five intervals between the six concentrations. AUC values were calculated independently for each NP and bacterial strain over the same concentration range. Higher AUC values indicated greater integrated biofilm biomass reduction across the tested concentrations.

The analysis was based on the concentration-specific biomass reduction percentages reported in the experimental results. Accordingly, the resulting AUC values were considered descriptive measures of the overall concentration–response profiles. Differences between AUC values were not interpreted as statistically significant in the absence of replicate-level AUC analysis. Furthermore, because crystal violet staining quantifies retained biofilm biomass rather than viable bacterial counts, the calculated AUC values were not interpreted as measures of bacterial killing, biofilm eradication, or NP penetration into the biofilm matrix. This distinction is consistent with established methodological considerations for quantitative biofilm analysis [2].

4.10. Statistical Analysis

Quantitative data are presented as mean ± standard deviation (SD) from triplicate experiments. Statistical analyses were performed using GraphPad Prism 8 following assessment of data normality. One-way ANOVA with Tukey's post hoc test was used for comparisons among NPs, while two-way ANOVA with Tukey's multiple comparisons test was applied to antibiofilm (NP × concentration) and time-kill (treatment × time) data. MIC values were reported descriptively.

Drug-content-normalized MIC, MIC fold-change, and MIC-normalized time-kill exposure ratios were calculated and evaluated descriptively. Antibiofilm concentration–response AUC values were determined using the trapezoidal rule over $\log_{10}$-transformed concentrations (15.62–500 µg/mL). As AUC values were derived from group means, no additional statistical testing was performed. Statistical significance was set at $p < 0.05$.

5. Conclusions

CA-loaded Eudragit® RS100/RL100 nanoparticles (NPs) were successfully prepared using nano spray drying, with polymer composition and drug-to-polymer ratio influencing their physicochemical and microbiological characteristics. FT-IR and ^{1}H-NMR analyses indicated no new covalent interactions. All drug-loaded NPs exhibited antibacterial activity, whereas blank NPs were inactive. Drug-content-normalized MIC analysis confirmed the greater planktonic potency of free CA, while NP-1 showed the most favorable MIC profile among the NPs. MIC-normalized time-kill analysis revealed NP-dependent exposure differences, with bacterial growth suppression predominating over bactericidal activity. All NPs reduced pre-established *Staphylococcus aureus* and *Escherichia coli* biofilm biomass, with NP-6 exhibiting the highest numerical concentration–response AUC values against both strains. However, these findings did not establish statistical superiority, bacterial killing, or biofilm eradication. Overall, the developed NPs demonstrated NP-dependent microbiological performance rather than superiority over free CA. Further studies involving drug-release kinetics, drug-equivalent comparisons, biofilm viability, and biocompatibility are required to establish their potential as antibiotic delivery systems.

Author Contributions: Conceptualization, P.S. and A.A.Ö.; methodology, P.S., A.A.Ö., T.Ç. and U.M.G.B.; investigation, P.S., A.A.Ö., T.Ç. and U.M.G.B.; data curation, P.S.; formal analysis, P.S., T.Ç. and U.M.G.B.; visualization, P.S.; validation, P.S., A.A.Ö., T.Ç. and U.M.G.B.; resources, P.S. and A.A.Ö.; supervision, A.A.Ö.; project administration, A.A.Ö.; funding acquisition, A.A.Ö.; writing—original draft preparation, P.S.; writing—review and editing, P.S. and A.A.Ö. All authors have read and agreed to the published version of the manuscript.

Funding: This research was funded by the Scientific Research Projects Commission of Anadolu University under Project No. YTT-2025-3144 and by the Rapid Support Project No. 3686.

Institutional Review Board Statement: Not applicable. This study did not involve human participants or experimental animals.

Informed Consent Statement: Not applicable.

Data Availability Statement: The data supporting the findings of this study are available from the corresponding author upon reasonable request.

Acknowledgments: The authors gratefully acknowledge Anadolu University for financial support provided through the Scientific Research Projects Commission.

Conflicts of Interest: The authors declare no conflicts of interest.

Abbreviations

The following abbreviations are used in this manuscript:

CA	Cefuroxime axetil
CFU	Colony-forming unit
CLSI	Clinical and Laboratory Standards Institute
DLS	Dynamic light scattering
ELS	Electrophoretic light scattering
Eudragit® RL 100	ERL 100
Eudragit® RS 100	ERS 100
FT-IR	Fourier-transform infrared spectroscopy
MHA	Mueller–Hinton agar
MHB	Mueller–Hinton broth
MIC	Minimum inhibitory concentration
NMR	Nuclear magnetic resonance
NP	Nanoparticle

OD	Optical density
PBS	Phosphate-buffered saline
PDI	Polydispersity index
PS	Particle size
RL100	Eudragit® RL100
RS100	Eudragit® RS100
SD	Standard deviation
UV-Vis	Ultraviolet-visible spectroscopy
ZP	Zeta potential
^{1}H-NMR	Proton nuclear magnetic resonance

References

1. Cheow, W.S.; Hadinoto, K. Antibiotic Polymeric Nanoparticles for Biofilm-Associated Infection Therapy. *Methods Mol. Biol.* **2014**, *1147*, 227–238. [CrossRef] [PubMed]
2. Li, C.; Cornel, E.J.; Du, J. Advances and Prospects of Polymeric Particles for the Treatment of Bacterial Biofilms. *ACS Appl. Polym. Mater.* **2021**, *3*, 2218–2232. [CrossRef]
3. Chen, Y.; Huang, Y.; Jin, Q. Polymeric Nanoplatforms for the Delivery of Antibacterial Agents. *Macromol. Chem. Phys.* **2022**, *223*, 2100440. [CrossRef]
4. Spirescu, V.A.; Chircov, C.; Grumezescu, A.M.; Andronescu, E. Polymeric Nanoparticles for Antimicrobial Therapies: An up-to-Date Overview. *Polymers* **2021**, *13*, 724. [CrossRef] [PubMed]
5. Bilensoy, E. Nanopartiküller. In *Nanofarmasötikler ve Uygulamaları*; Zırh Gürsoy, A., Ed.; Kontrollü Salım Sistemleri Derneği Yayını: İstanbul, Türkiye, 2014; pp. 23–39.
6. Mudshinge, S.R.; Deore, A.B.; Patil, S.; Bhalgat, C.M. Nanoparticles: Emerging Carriers for Drug Delivery. *Saudi Pharm. J.* **2011**, *19*, 129–141. [CrossRef] [PubMed]
7. Nagarwal, R.C.; Kant, S.; Singh, P.N.; Maiti, P.; Pandit, J.K. Polymeric Nanoparticulate System: A Potential Approach for Ocular Drug Delivery. *J. Control. Release* **2009**, *136*, 2–13. [CrossRef] [PubMed]
8. Gelperina, S.; Kisich, K.; Iseman, M.D.; Heifets, L. The Potential Advantages of Nanoparticle Drug Delivery Systems in Chemotherapy of Tuberculosis. *Am. J. Respir. Crit. Care Med.* **2005**, *172*, 1487–1490. [CrossRef] [PubMed]
9. Kaş, H.S. İlaç Taşıyıcı Partiküler Sistemler. In *Kontrollü salım sistemleri*; Zırh Gürsoy, A., Ed.; Kontrollü Salım Sistemleri Derneği Yayını: İstanbul, Türkiye, 2002; pp. 65–102.
10. Pandey, H.; Sharma, U.K.; Pandey, A.C. Eudragit-Based Nanostructures: A Potential Approach for Ocular Drug Delivery. *Int. J. Res. Dev. Pharm. Life Sci.* **2012**, *1*, 40–43.
11. Nikam, A.; Sahoo, P.R.; Musale, S.; Pagar, R.R.; Paiva-Santos, A.C.; Giram, P.S. A Systematic Overview of Eudragit® Based Copolymer for Smart Healthcare. *Pharmaceutics* **2023**, *15*, 587. [CrossRef] [PubMed]
12. Kumari, A.; Yadav, S.K.; Yadav, S.C. Biodegradable Polymeric Nanoparticles Based Drug Delivery Systems. *Colloids Surf. B Biointerfaces* **2010**, *75*, 1–18. [CrossRef] [PubMed]
13. Bürki, K.; Jeon, I.; Arpagaus, C.; Betz, G. New Insights into Respirable Protein Powder Preparation Using a Nano Spray Dryer. *Int. J. Pharm.* **2011**, *408*, 248–256. [CrossRef] [PubMed]
14. Gharsallaoui, A.; Roudaut, G.; Chambin, O.; Voilley, A.; Saurel, R. Applications of Spray-Drying in Microencapsulation of Food Ingredients: An Overview. *Food Res. Int.* **2007**, *40*, 1107–1121. [CrossRef]
15. Celli, G.B.; Ghanem, A.; Brooks, M.S.-L. Bioactive Encapsulated Powders for Functional Foods—A Review of Methods and Current Limitations. *Food Bioproc. Tech.* **2015**, *8*, 1825–1837. [CrossRef]
16. Arpagaus, C.; Collenberg, A.; Rütti, D.; Assadpour, E.; Jafari, S.M. Nano Spray Drying for Encapsulation of Pharmaceuticals. *Int. J. Pharm.* **2018**, *546*, 194–214. [CrossRef] [PubMed]
17. Heng, D.; Lee, S.H.; Ng, W.K.; Tan, R.B. The Nano Spray Dryer B-90. *Expert Opin. Drug Deliv.* **2011**, *8*, 965–972. [CrossRef] [PubMed]
18. Tshweu, L.; Katata, L.; Kalombo, L.; Swai, H. Nanoencapsulation of Water-Soluble Drug, Lamivudine, Using a Double Emulsion Spray-Drying Technique for Improving HIV Treatment. *J. Nanoparticle Res.* **2013**, *15*, 1–11. [CrossRef]
19. Šeremet, D.; Tuzla, B.; Vrsaljko, D.; Vukosav, P.; Mišić Radić, T.; Kuzmić, S.; Žižek, K.; Sokač, K.; Mandura Jarić, A.; Vojvodić Cebin, A.; et al. Development of New Chocolate Formulations by Incorporating Spray-Dried and Liposomal Encapsulates of Ground Ivy (*Glechoma hederacea* L.) Polyphenolic Extract. *Food Chem.* **2025**, *480*, 143907. [CrossRef] [PubMed]
20. Schulze, J.; Kuhn, S.; Hendrikx, S.; Schulz-Siegmund, M.; Polte, T.; Aigner, A. Spray-dried Nanoparticle-in-microparticle Delivery Systems (Nimds) for Gene Delivery, Comprising Polyethylenimine (Pei)-based Nanoparticles in a Poly (Vinyl Alcohol) Matrix. *Small* **2018**, *14*, 1701810. [CrossRef] [PubMed]

21. Vehring, R. Pharmaceutical Particle Engineering via Spray Drying. *Pharm. Res.* **2008**, *25*, 999–1022. [CrossRef] [PubMed]
22. Lee, S.H.; Heng, D.; Ng, W.K.; Chan, H.-K.; Tan, R.B.H. Nano Spray Drying: A Novel Method for Preparing Protein Nanoparticles for Protein Therapy. *Int. J. Pharm.* **2011**, *403*, 192–200. [CrossRef] [PubMed]
23. Stavras, F.-M.; Partheniadis, I.; Nikolakakis, I. Formulation of Taste-Masked Orodispersible Famotidine Tablets by Sequential Spray Drying and Direct Compression–Bitterness Evaluation. *J. Drug Deliv. Sci. Technol.* **2023**, *81*, 104290. [CrossRef]
24. Gangurde, A.B.; Amin, P.D. Microencapsulation by Spray Drying of Vitamin A Palmitate from Oil to Powder and Its Application in Topical Delivery System. *J. Encapsulation Adsorpt. Sci.* **2017**, *7*, 10.
25. Soyer, P.; Öztürk, A.A. Comparative Evaluation of Extrusion and Emulsification Techniques for Alginate-Based Microencapsulation of *Bifidobacterium longum*. *Fabad J. Pharm. Sci.* **2026**, *51*, 853–864. [CrossRef]
26. Xiong, M.H.; Bao, Y.; Yang, X.Z.; Zhu, Y.H.; Wang, J. Delivery of Antibiotics with Polymeric Particles. *Adv. Drug Deliv. Rev.* **2014**, *78*, 63–76. [CrossRef] [PubMed]
27. Choi, V.; Rohn, J.L.; Stoodley, P.; Carugo, D.; Stride, E. Drug Delivery Strategies for Antibiofilm Therapy. *Nat. Rev. Microbiol.* **2023**, *21*, 555–572. [CrossRef] [PubMed]
28. Shah, P.M. Classification of Oral Cephalosporins. *Int. J. Antimicrob. Agents* **2002**, *19*, 163–164. [CrossRef] [PubMed]
29. Dabrowska, M.; Krzek, J. Chiral Separation of Diastereoisomers of Cefuroxime Axetil by High-Performance Thin-Layer Chromatography. *J. AOAC Int.* **2010**, *93*, 771–777. [CrossRef]
30. Jammula, S.; Patra, C.N.; Swain, S.; Panigrahi, K.C.; Nayak, S.; Dinda, S.C.; Rao, M.E.B. Design and Characterization of Cefuroxime Axetil Biphasic Floating Minitablets. *Drug Deliv.* **2015**, *22*, 125–135. [CrossRef] [PubMed]
31. Erdoğan Kablan, S. *Sefuroksim Aksetilin Voltametrik Davranışlarının Incelenmesi ve Elektroanalitik Yöntemlerle Farmasötik Preparatlardan Analizi*; Yüksek Lisans, Hacettepe Üniversitesi Sağlık Bilimleri Enstitüsü: Ankara, Türkiye, 2015.
32. Akova, M.; Kayaalp, O. Beta-Laktam Antibiyotikler I-Penisilinler. In *Tıbbi Farmakoloji*; Kayaalp, O., Ed.; Pelikan Yayıncılık: Ankara, Türkiye, 2009; pp. 167–188.
33. Akova, M.; Kayaalp, O. Beta-laktam antibiyotikler II-Sefalosporinler ve diğerleri. In *Tıbbi Farmakoloji*; Kayaalp, O., Ed.; Pelikan Yayıncılık: Ankara, Türkiye, 2009; pp. 188–200.
34. Melli, M.; Kayaalp, O. Kemoterapötiklere giriş, İnfeksiyon tedavisinin farmakolojik ve farmakokinetik esasları. In *Tıbbi Farmakoloji*; Kayaalp, O., Ed.; Pelikan Yayıncılık: Ankara, Türkiye, 2009; pp. 144–166.
35. Rowe, R.C.; Seskey, P.J.; Quinn, M.E. *Handbook of Pharmaceutical Excipients*; Pharmaceutical Press: Chicago, IL, USA, 2009.
36. Pignatello, R.; Ferro, M.; Puglisi, G. Preparation of Solid Dispersions of Nonsteroidal Anti-Inflammatory Drugs with Acrylic Polymers and Studies on Mechanisms of Drug-Polymer Interactions. *AAPS PharmSciTech* **2002**, *3*, 35–45. [CrossRef] [PubMed]
37. Pignatello, R.; Bucolo, C.; Puglisi, G. Ocular Tolerability of Eudragit RS100® and RL100® Nanosuspensions as Carriers for Ophthalmic Controlled Drug Delivery. *J. Pharm. Sci.* **2002**, *91*, 2636–2641. [CrossRef] [PubMed]
38. Hadinoto, K.; Cheow, W.S. Nano-Antibiotics in Chronic Lung Infection Therapy against Pseudomonas Aeruginosa. *Colloids Surf. B Biointerfaces* **2014**, *116*, 772–785. [CrossRef] [PubMed]
39. Joshi, M. Role of Eudragit in Target Drug Delivery. *Int. J. Curr. Pharm. Res.* **2013**, *5*, 58–62.
40. El-Nahas, A.E.; Allam, A.N.; Abdelmonsif, D.A.; El-Kamel, A.H. Silymarin-Loaded Eudragit Nanoparticles: Formulation, Characterization, and Hepatoprotective and Toxicity Evaluation. *AAPS PharmSciTech* **2017**, *18*, 3076–3086. [CrossRef] [PubMed]
41. Dhumal, R.S.; Biradar, S.V.; Aher, S.; Paradkar, A.R. Cefuroxime Axetil Solid Dispersion with Polyglycolized Glycerides for Improved Stability and Bioavailability. *J. Pharm. Pharmacol.* **2009**, *61*, 743–751. [CrossRef] [PubMed]
42. Schmid, K.; Arpagaus, C.; Friess, W. Evaluation of the Nano Spray Dryer B-90 for Pharmaceutical Applications. *Pharm. Dev. Technol.* **2011**, *16*, 287–294. [CrossRef] [PubMed]
43. Salatin, S.; Barar, J.; Barzegar-Jalali, M.; Adibkia, K.; Kiafar, F.; Jelvehgari, M. Development of a Nanoprecipitation Method for the Entrapment of a Very Water Soluble Drug into Eudragit RL Nanoparticles. *Res. Pharm. Sci.* **2017**, *12*, 1. [CrossRef] [PubMed]
44. Danaei, M.; Dehghankhold, M.; Ataei, S.; Hasanzadeh Davarani, F.; Javanmard, R.; Dokhani, A.; Khorasani, S.; Mozafari, M.R. Impact of Particle Size and Polydispersity Index on the Clinical Applications of Lipidic Nanocarrier Systems. *Pharmaceutics* **2018**, *10*, 57. [CrossRef] [PubMed]
45. Honary, S.; Zahir, F. Effect of Zeta Potential on the Properties of Nano-Drug Delivery Systems-a Review (Part 1). *Trop. J. Pharm. Res.* **2013**, *12*, 255–264. [CrossRef]
46. Mishra, B.; Patel, B.B.; Tiwari, S. Colloidal Nanocarriers: A Review on Formulation Technology, Types and Applications toward Targeted Drug Delivery. *Nanomedicine* **2010**, *6*, 9–24. [CrossRef] [PubMed]
47. Pignatello, R.; Ferro, M.; De Guidi, G.; Salemi, G.; Vandelli, M.A.; Guccione, S.; Geppi, M.; Forte, C.; Puglisi, G. Preparation, Characterisation and Photosensitivity Studies of Solid Dispersions of Diflunisal and Eudragit RS100® and RL100®. *Int. J. Pharm.* **2001**, *218*, 27–42. [CrossRef] [PubMed]
48. Ficarra, R.; Tommasini, S.; Raneri, D.; Calabro, M.L.; Di Bella, M.R.; Rustichelli, C.; Gamberini, M.C.; Ficarra, P. Study of Flavonoids/β-Cyclodextrins Inclusion Complexes by NMR, FT-IR, DSC, X-Ray Investigation. *J. Pharm. Biomed. Anal.* **2002**, *29*, 1005–1014. [CrossRef] [PubMed]

49. Sun, J.; Walker, J.; Beck-Broichsitter, M.; Schwendeman, S.P. Characterization of Commercial PLGAs by NMR Spectroscopy. *Drug Deliv. Transl. Res.* **2022**, *12*, 720–729, Correction in *Drug Deliv. Transl. Res.* **2022**, *12*, 730. https://doi.org/10.1007/s13346-021-01061-x. [CrossRef] [PubMed]
50. Güven, U.M.; Başaran, E. In Vitro-in Vivo Evaluation of Olopatadine Incorporated Chitosan Nanoparticles for the Treatment of Ocular Allergy. *J. Drug Deliv. Sci. Technol.* **2021**, *64*, 102518. [CrossRef]
51. Cannavà, C.; Crupi, V.; Guardo, M.; Majolino, D.; Stancanelli, R.; Tommasini, S.; Ventura, C.A.; Venuti, V. Phase Solubility and FTIR-ATR Studies of Idebenone/Sulfobutyl Ether β-Cyclodextrin Inclusion Complex. *J. Incl. Phenom. Macrocycl. Chem.* **2013**, *75*, 255–262. [CrossRef]
52. Stancanelli, R.; Ficarra, R.; Cannavà, C.; Guardo, M.; Calabrò, M.L.; Ficarra, P.; Ottanà, R.; Maccari, R.; Crupi, V.; Majolino, D. UV–Vis and FTIR-ATR Characterization of 9-Fluorenon-2-Carboxyester/(2-Hydroxypropyl)-β-Cyclodextrin Inclusion Complex. *J. Pharm. Biomed. Anal.* **2008**, *47*, 704–709. [CrossRef] [PubMed]
53. Rojek, B.; Bartyzel, A.; Sawicki, W.; Plenis, A. DSC, TGA-FTIR and FTIR Assisted by Chemometric Factor Analysis and PXRD in Assessing the Incompatibility of the Antiviral Drug Arbidol Hydrochloride with Pharmaceutical Excipients. *Molecules* **2024**, *29*, 264. [CrossRef] [PubMed]
54. Lin, S.-Y. Current and Potential Applications of Simultaneous DSC-FTIR Microspectroscopy for Pharmaceutical Analysis. *J. Food Drug Anal.* **2021**, *29*, 182–202. [CrossRef] [PubMed]
55. Birk, S.E.; Boisen, A.; Nielsen, L.H. Polymeric Nano- and Microparticulate Drug Delivery Systems for Treatment of Biofilms. *Adv. Drug Deliv. Rev.* **2021**, *174*, 30–52. [CrossRef] [PubMed]
56. Wiegand, I.; Hilpert, K.; Hancock, R.E.W. Agar and Broth Dilution Methods to Determine the Minimal Inhibitory Concentration (MIC) of Antimicrobial Substances. *Nat. Protoc.* **2008**, *3*, 163–175. [CrossRef] [PubMed]
57. Balouiri, M.; Sadiki, M.; Ibnsouda, S.K. Methods for in Vitro Evaluating Antimicrobial Activity: A Review. *J. Pharm. Anal.* **2016**, *6*, 71–79. [CrossRef] [PubMed]
58. Ciofu, O.; Moser, C.; Jensen, P.Ø.; Høiby, N. Tolerance and Resistance of Microbial Biofilms. *Nat. Rev. Microbiol.* **2022**, *20*, 621–635. [CrossRef] [PubMed]
59. Flemming, H.C.; van Hullebusch, E.D.; Neu, T.R.; Nielsen, P.H.; Seviour, T.; Stoodley, P.; Wingender, J.; Wuertz, S. The Biofilm Matrix: Multitasking in a Shared Space. *Nat. Rev. Microbiol.* **2022**, *21*, 70–86. [CrossRef] [PubMed]
60. Hall, C.W.; Mah, T.F. Molecular Mechanisms of Biofilm-Based Antibiotic Resistance and Tolerance in Pathogenic Bacteria. *FEMS Microbiol. Rev.* **2017**, *41*, 276–301. [CrossRef] [PubMed]
61. Azeredo, J.; Azevedo, N.F.; Briandet, R.; Cerca, N.; Coenye, T.; Costa, A.R.; Desvaux, M.; Di Bonaventura, G.; Hébraud, M.; Jaglic, Z.; et al. Critical Review on Biofilm Methods. *Crit. Rev. Microbiol.* **2017**, *43*, 313–351. [CrossRef] [PubMed]
62. Haney, E.F.; Trimble, M.J.; Hancock, R.E.W. Microtiter Plate Assays to Assess Antibiofilm Activity against Bacteria. *Nat. Protoc.* **2021**, *16*, 2615–2632. [CrossRef] [PubMed]
63. Dillen, K.; Vandervoort, J.; Van den Mooter, G.; Ludwig, A. Evaluation of Ciprofloxacin-Loaded Eudragit® RS100 or RL100/PLGA Nanoparticles. *Int. J. Pharm.* **2006**, *314*, 72–82. [CrossRef] [PubMed]
64. Forier, K.; Raemdonck, K.; De Smedt, S.C.; Demeester, J.; Coenye, T.; Braeckmans, K. Lipid and Polymer Nanoparticles for Drug Delivery to Bacterial Biofilms. *J. Control. Release* **2014**, *190*, 607–623. [CrossRef] [PubMed]
65. Magana, M.; Sereti, C.; Ioannidis, A.; Mitchell, C.A.; Ball, A.R.; Magiorkinis, E.; Chatzipanagiotou, S.; Hamblin, M.R.; Hadjifrangiskou, M.; Tegos, G.P. Options and Limitations in Clinical Investigation of Bacterial Biofilms. *Clin. Microbiol. Rev.* **2018**, *31*, e00084-16. [CrossRef] [PubMed]
66. Guideline, I.C.H.H. *Validation of Analytical Procedures Q2 (R2)*; ICH: Geneva, Switzerland, 2022.
67. Çevikelli, T.; Güven, U.M.; Öztürk, A.A. Metronidazole Loaded Novel Microemulsion Formulation for Topical Delivery and Characterization With Validated New UPLC Method. *Fabad J. Pharm. Sci.* **2024**, *49*, 111–128. [CrossRef]
68. Öztürk, A.A.; Yenilmez, E.; Yazan, Y. Development and Validation of High Performance Liquid Chromatography (HPLC) Modified Method for Dexketoprofen Trometamol. *Eur. Int. J. Sci. Technol.* **2017**, *6*, 33–41.
69. Korany, M.A.; Haggag, R.S.; Ragab, M.A.A.; Elmallah, O.A. A Validated Stability-Indicating HPLC Method for Simultaneous Determination of Silymarin and Curcumin in Various Dosage Forms. *Arab. J. Chem.* **2017**, *10*, S1711–S1725. [CrossRef]
70. Yasir, M.; Singh Sara, U.V.; Chauhan, I.; Bisht, D.; Puri, D.; Maurya, J. Donepezil Base: Physicochemical Characterization, HPLC Method Development, Validation and Its Application for the Determination of Shelf Life in Developed Solid Lipid Nanoparticles. *Curr. Nanomed. Former. Recent Pat. Nanomed.* **2020**, *10*, 48–62. [CrossRef]
71. Migues, V.H.; David, J.M.; Gomes, A.F.; David, J.P. Determination of Soybean Isoflavone by HPLC/DAD and Simple UV Spectroscopic Analysis: A Comparative Study. *Food Anal. Methods* **2022**, *15*, 367–376. [CrossRef]
72. Mendez, A.S.L.; Steppe, M.; Schapoval, E.E.S. Validation of HPLC and UV Spectrophotometric Methods for the Determination of Meropenem in Pharmaceutical Dosage Form. *J. Pharm. Biomed. Anal.* **2003**, *33*, 947–954. [CrossRef] [PubMed]

73. Nakashima, K.; Itoh, K.; Kono, M.; Nakashima, M.N.; Wada, M. Determination of Donepezil Hydrochloride in Human and Rat Plasma, Blood and Brain Microdialysates by HPLC with a Short C30 Column. *J. Pharm. Biomed. Anal.* **2006**, *41*, 201–206. [CrossRef] [PubMed]
74. Li, X.; Anton, N.; Arpagaus, C.; Belleteix, F.; Vandamme, T.F. Nanoparticles by Spray Drying Using Innovative New Technology: The Büchi Nano Spray Dryer B-90. *J. Control. Release* **2010**, *147*, 304–310. [CrossRef] [PubMed]
75. Hoşer, H.C.; Soyer, P.; Tilki, E.K.; Arısoy, S.; Alper Öztürk, A. CQA and DoE Guided Development of Brimonidine Tartrate Loaded Polymeric Nanoparticles for Sustained Ocular Delivery and in Vitro Neuroprotective Evaluation in Glaucoma. *J. Drug Deliv. Sci. Technol.* **2026**, *123*, 108568. [CrossRef]
76. Solak, B.; Soyer, P.; Kaya-Tilki, E.; Öztürk, A.A. Evaluation of Antimicrobial Properties and Antioxidant Activity of Rosmarinic Acid Loaded Resomer RG 502 H Based Nanoparticles against Tert-Butyl Hydroperoxide-Induced Oxidative Stress: A Detailed Formulation, Characterization and Efficacy Determination Study. *J. Drug Deliv. Sci. Technol.* **2025**, *106*, 106721. [CrossRef]
77. Kurban, B.; Tuncel, T.; Görgülü, Ş.; Kar, F.; Öztürk, A.; Özek, T. Elemi Essential Oil Nanocapsulated Drug Ameliorates Lung Cancer via Oxidative Stress, Apoptosis and Inflammation Pathway. *J. Cell. Mol. Med.* **2023**, *27*, 1887–1899. [CrossRef] [PubMed]
78. Çevikelli, T.; Güven Bölgen, U.M.; Öztürk, A.A.; Kandır, S.; Balcı Özyurt, A.; Akyüz-Çetin, S.; Çelenk, A.; Eroğlu Özkan, E.; Demirci Kayıran, S. Lavandula Angustifolia and Pinus Brutia Loaded Nanoemulsion Enhances In Vivo Burn Wound Healing: Histopathological and Cytokine-Based Mechanistic Evidence. *J. Drug Deliv. Sci. Technol.* **2026**, *122*, 108372. [CrossRef]
79. Öztürk, A.A.; Güven, U.M.; Yenilmez, E. Flurbiprofen Loaded Gel Based Topical Delivery System: Formulation and in Vitro Characterization with New Developed Uplc Method. *ACTA Pharm. Sci.* **2018**, *56*, 81. [CrossRef]
80. Kömür, M.; Kıyan, H.T.; Öztürk, A.A. Development of Donepezil Hydrochloride-Loaded PLGA-Based Nanoparticles for Alzheimer's Disease Treatment. *Sci. Rep.* **2025**, *15*, 13184. [CrossRef] [PubMed]
81. Arınmış, K.N.; Kıyan, H.T.; Öztürk, A.A. Preparation, Characterization, Antioxidant Activities, and Determination of Anti-Alzheimer Effects of PLGA-Based DDSs Containing Ferulic Acid. *ACS Omega* **2024**, *9*, 11321–11338. [CrossRef] [PubMed]
82. Altıntop, M.D.; Çiftçi, K.; Şentürk, M.K.; Öztürk, A.A.; Altınpulluk, H.; Ertorun, İ.; Akalın Çiftçi, G. Development of a New Series of Thiazoles as EGFR-Targeted Anticancer Agents for NSCLC Therapy through Nanotechnological and Computer-Aided Approaches. *Bioorg. Chem.* **2026**, *178*, 109938. [CrossRef] [PubMed]
83. Şahin, Ş.; Kaya-Tilki, E.; Baysal, M.; Öztürk, A.A. Preparation and Evaluation of Temozolomide Loaded PLGA Nanoparticles for the Treatment of Glioblastoma Multiforme. *Sci. Rep.* **2025**, *15*, 36194. [CrossRef] [PubMed]
84. Soyer, P.; Öztürk, A.A. Development and Functional Evaluation of a Pharmabiotic Food Supplement Containing Microencapsulated *Lactiplantibacillus pentosus* for Oral Microbiome Health. *Food Sci. Nutr.* **2026**, *14*, e72243. [CrossRef] [PubMed]
85. Karakaya, A.; Bağcı, E.R.; Soyer, P.; Daoud, N.E.H.; Erçetin, T.; Acar Çevik, U. Synthesis, In Vitro Antimicrobial, and Antioxidant Activities of Novel Thiazole Derivatives. *Chem. Biodivers.* **2026**, *23*, e03308. [CrossRef] [PubMed]
86. Barry, A.L.; Craig, W.A.; Nadler, H.; Reller, L.B.; Sanders, C.C.; Swenson, J.M. CLSI M26: Methods for Determining Bactericidal Activity of Antimicrobial Agents. *CLSI* **1999**, *1*, 1–32.
87. Stepanović, S.; Vuković, D.; Hola, V.; Di Bonaventura, G.; Djukić, S.; Ćirković, I.; Ruzicka, F. Quantification of Biofilm in Microtiter Plates: Overview of Testing Conditions and Practical Recommendations for Assessment of Biofilm Production by Staphylococci. *APMIS* **2007**, *115*, 891–899. [CrossRef] [PubMed]
88. Kaya, B.; Acar Çevik, U.; Soyer, P.; Yıldız, M.T.; Özkay, Y.; Kaplancıklı, Z.A. Design and Synthesis of New 1,3,4-Thiadiazoles as Antimicrobial and Antibiofilm Agents. *Z. Fur Naturforschung Sect. C J. Biosci.* **2025**, *80*, 719–726. [CrossRef] [PubMed]
89. Öğüt, K.; Soyer, P. Evaluation of Antimicrobial and Biofilm Inhibitory Activities of Flower, Leaf, Seed, and Pulp Extracts of *Mahonia aquifolium* (Pursh) Nutt. *Fabad J. Pharm. Sci.* **2026**, *51*, 755–766. [CrossRef]
90. Soyer, P.; Öztürk, A.A. Development of Pharmabiotic Gel-Serums with *Lacticaseibacillus casei* Postbiotics and Paraprobiotics Using Chitosan and Carbopol. *Gels* **2026**, *12*, 838. [CrossRef] [PubMed]

Disclaimer/Publisher's Note: The statements, opinions and data contained in all publications are solely those of the individual author(s) and contributor(s) and not of MDPI and/or the editor(s). MDPI and/or the editor(s) disclaim responsibility for any injury to people or property resulting from any ideas, methods, instructions or products referred to in the content.